Dynamics of chemical equilibrium of hadronic matter close to T_c

J. Noronha-Hostler,[1] M. Beitel,[2] C. Greiner,[2] and I. Shovkovy[3]
[1]*The Frankfurt International Graduate School for Science (FIGSS), D-60438 Frankfurt am Main, Germany*
[2]*Institut für Theoretische Physik, Johann Wolfgang Goethe-Universität, D-60438 Frankfurt am Main, Germany*
[3]*Department of Applied Sciences and Mathematics, Arizona State University, Mesa, Arizona 85212, USA*
(Received 29 October 2009; published 28 May 2010)

Quick chemical equilibration times of hadrons (specifically, $p\bar{p}$, $K\bar{K}$, $\Lambda\bar{\Lambda}$, and $\Omega\bar{\Omega}$ pairs) within a hadron gas are explained dynamically using Hagedorn states, which drive particles into equilibrium close to the critical temperature. Within this scheme, we use master equations and derive various analytical estimates for the chemical equilibration times. We compare our model to recent lattice results and find that for both $T_c = 176$ MeV and $T_c = 196$ MeV, the hadrons can reach chemical equilibrium almost immediately, well before the chemical freeze-out temperatures found in thermal fits for a hadron gas without Hagedorn states. Furthermore, the ratios p/π, K/π, Λ/π, and Ω/π match experimental values well in our dynamical scenario.

DOI: 10.1103/PhysRevC.81.054909 PACS number(s): 25.75.Gz, 24.30.−v

I. INTRODUCTION

(Anti-)strangeness enhancement was first observed at CERN-SPS energies by comparing antihyperons, multistrange baryons, and kaons to pp data. It was considered a signature for quark gluon plasma (QGP) because, using binary strangeness production and exchange reactions, chemical equilibrium could not be reached within a standard hadron gas phase; that is, the chemical equilibration time was on the order of $\tau \sim 100$–1000 fm/c, whereas the lifetime of a fireball in the hadronic stages is only $\tau \approx 4$–7 fm/c [1]. It was then proposed that there exists a strong hint for QGP at SPS because strange quarks can be produced more abundantly by gluon fusion, which would account for strangeness enhancement following hadronization and rescattering of strange quarks. Later, however, multimesonic reactions were used to explain secondary production of $\bar{p}$ and antihyperons [2,3]. At SPS they give a chemical equilibration time of $\tau_{\bar{Y}} \approx 1$–3 fm/c using an annihilation cross section of $\sigma_{\rho\bar{Y}} \approx \sigma_{\rho\bar{p}} \approx 50$ mb and a baryon density of $\rho_B \approx \rho_0$ to $2\rho_0$, which is typical for evolving strongly interacting matter at SPS before chemical freeze-out. Therefore, the time scale is short enough to account for chemical equilibration within a cooling hadronic fireball at SPS.

A problem arises when the same multimesonic reactions were employed in the hadron gas phase at RHIC temperatures where experiments again show that the particle abundances reach chemical equilibration close to the phase transition [4]. At RHIC at $T = 170$ MeV, where $\sigma \approx 30$ mb and $\rho_B^{\rm eq} \approx \rho_{\bar{B}}^{\rm eq} \approx 0.04$ fm^{-3}, the equilibrium rate for (anti-)baryon production is $\tau \approx 10$ fm/c.

Moreover, $\tau \approx 10$ fm/c was also obtained in Ref. [5] using a fluctuation-dissipation theorem. From hadron cascades a significant deviation was found from the chemically saturated strange (anti-)baryons yields in the 5% most central Au-Au collisions [6]. These discrepancies suggest that hadrons are "born" into equilibrium; that is, the system is already in a chemically frozen-out state at the end of the phase transition [7,8]. To circumvent such long time scales, it was suggested that near T_c there exists an extralarge particle density overpopulated with pions and kaons, which drive the baryons and anti-baryons into equilibrium [9]. However, it is not clear how this overpopulation should appear, and how the subsequent population of (anti-)baryons would follow. Moreover, the overpopulated (anti-)baryons do not later disappear [10]. Therefore, it was conjectured that Hagedorn resonances (heavy resonances near T_c with an exponential mass spectrum) could account for the extra (anti-)baryons [10–12].

Hadrons can develop according to

$$n\pi \leftrightarrow \mathrm{HS} \leftrightarrow n'\pi + X\bar{X}, \tag{1}$$

where $X\bar{X}$ can be substituted with $p\bar{p}$, $K\bar{K}$, $\Lambda\bar{\Lambda}$, or $\Omega\bar{\Omega}$. Equation (1) provides an efficient method for producing of $X\bar{X}$ pairs because of the large decay widths of the Hagedorn states. In Eq. (1), n is the number of pions for the decay $n\pi \leftrightarrow$ HS and n' is the number of pions that a Hagedorn state will decay into when an $X\bar{X}$ is present. Because Hagedorn resonances are highly unstable, the phase space for multiparticle decays drastically increases when the mass increases. Therefore, the resonances catalyze rapid equilibration of $X\bar{X}$ near T_c and die out moderately below T_c [11].

Unlike in pure glue SU(3) gauge theory where the Polyakov loop is the order parameter for the deconfinement transition (which is weakly first order), the rapid crossover seen on lattice calculations involving dynamical fermions indicates that there is not a well-defined order parameter that can distinguish the confined phase from the deconfined phase. Because of this, it is natural to look for a hadronic mechanism for quick chemical equilibration near the phase transition. One such possibility could be the inclusion of Hagedorn states. Recently, Hagedorn states have been shown to contribute to the physical description of a hadron gas close to T_c. The inclusion of Hagedorn states leads to a low η/s in the hadron gas phase [13], which nears the string theory bound $\eta/s = 1/(4\pi)$ [14]. Calculations of the trace anomaly including Hagedorn states also fits recent lattice results well and correctly describe the minimum of the speed of sound squared, c_s^2, near the phase transition found on the lattice [13]. Estimates for the bulk viscosity including Hagedorn states in the hadron gas phase indicate that the bulk

viscosity, ζ/s, increases near T_c, which agrees with the general analysis done in [15]. Furthermore, it has been shown [16] that Hagedorn states provide a better fit within a thermal model to the hadron yield particle ratios. Additionally, Hagedorn states provide a mechanism to relate T_c and $T_{\rm chem}$, which then leads to the suggestion that a lower critical temperature could possibly be preferred, according to the thermal fits [16].

Previously, in Ref. [11] we presented analytical results, which we will derive in detail here. Moreover, we saw that both the baryons and the kaons equilibrated quickly within an expanding fireball. The initial saturation of pions, Hagedorn states, baryons, and kaons played no significant role in the ratios such as K/π and $(B+\bar{B})/\pi$.

Here we consider the effects of various initial conditions on the chemical freeze-out temperature and we find that while they play a small role in the total particle number, they still reproduce fast chemical equilibration times. Additionally, we assume lattice values of the critical temperatures ($T_c =$ 176 MeV [17] and $T_c = 196$ MeV [18,19]) and find that chemical equilibrium abundances are still reached close to the temperature given by thermal fits ($T \approx 160$ MeV).

This article is structured in the following manner. In Sec. II we discuss the details of our statistical model that calculates the chemical equilibrium values of the Hagedorn states and other hadrons. Furthermore, in this section, fits are shown to thermodynamical properties calculated in lattice QCD, which are used to determine the mass spectrum of the Hagedorn states, and the rate equations are discussed in detail. In Sec. III we are able to extract the chemical equilibration time of an $X\bar{X}$ pair when the pions and Hagedorn states are held constant. In Sec. IV we derive an analytical result of the rate equations when we consider only the decay HS $\leftrightarrow n\pi$. We then discuss the case of an expanding fireball and the results for the various $X\bar{X}$ pair production in Sec. V. The production of Ω particles will also be considered in Sec. VI. We summarize and discuss our results in Sec. VII. In the Appendix we present some analytical and numerical results for the various equilibration stages in the hadron and Hagedorn-states gas mixture.

II. MODEL

Hagedorn resonances have an exponentially growing mass spectrum [20]. Their large masses open up the phase space for multiparticle decays. Recent analysis involving Hagedorn states is given in Ref. [**?**]. Moreover, thoughts on observing Hagedorn states in experiments are given in Ref. [22] and their usage as a thermostat in Ref. [23]. Hagedorn states can also explain the phase transition *above* the critical temperature and, depending on the intrinsic parameters, the order of the phase transition [24]. For an application of Hagedorn states within hadronic jet events in e^+e^- collisions at CERN LEP, see Ref. [25].

For the following discussion, the overall density of Hagedorn states in our extended Hagedorn gas model are straightforwardly described by

$$\rho = \int_{M_0}^{M} \frac{A}{\left[m^2+m_r^2\right]^{\frac{5}{4}}} e^{\frac{m}{T_H}}\, dm, \tag{2}$$

where $M_0 = 2$ GeV and $m_r^2 = 0.5$ GeV. We note that in this work we consider only mesonic Hagedorn states with no net strangeness. The exponential in Eq. (2) arises from Hagedorn's original idea that there is an exponentially growing mass spectrum. Thus, as T_H is approached, Hagedorn states become increasingly more relevant and heavier resonances "appear." The factor in front of the exponential has various forms [**?**,23]. While the choice in this factor can vary, it was found in Ref. [**?**] that the present form gives lower values of T_H, which more closely match the predicted lattice critical temperature [17–19].

Returning to Eq. (2), its parameters (A, M, and T_H) are dependent on the critical temperature. We assume that $T_H = T_c$, and then we consider the two different different lattice results for T_c: $T_c = 196$ MeV [18,19], which uses an almost physical pion mass, and $T_c = 176$ MeV [17]. Furthermore, we need to take into account the repulsive interactions and, therefore, we use the following volume corrections (as also seen in [13,26,27]):

$$\begin{aligned}
T &= \frac{T^*}{1-\frac{p_{pt}(T^*,\,\mu_b^*)}{4B}},\\
\mu_b &= \frac{\mu_b^*}{1-\frac{p_{pt}(T^*,\,\mu_b^*)}{4B}},\\
p_{xv} &= \frac{p_{pt}(T^*,\,\mu_b^*)}{1-\frac{p_{pt}(T^*,\,\mu_b^*)}{4B}},\\
\varepsilon_{xv} &= \frac{\varepsilon_{pt}(T^*,\,\mu_b^*)}{1+\frac{\varepsilon_{pt}(T^*,\,\mu_b^*)}{4B}},\\
n_{xv} &= \frac{n_{pt}(T^*,\,\mu_b^*)}{1+\frac{\varepsilon_{pt}(T^*,\,\mu_b^*)}{4B}},\\
s_{xv} &= \frac{s_{pt}(T^*,\,\mu_b^*)}{1+\frac{\varepsilon_{pt}(T^*,\,\mu_b^*)}{4B}},
\end{aligned} \tag{3}$$

which ensure that the our model is thermodynamically consistent. Note that B is a free parameter that is based on the idea of the MIT bag constant.

To find the maximum Hagedorn-state mass M and the "degeneracy" A, we fit our model to the thermodynamic properties of the lattice. In the RBC-Bielefeld collaboration the thermodynamical properties are derived from the quantity $\varepsilon - 3p$, the so-called interaction measure, which is what we fit to obtain the parameters for the Hagedorn states. Thus, we obtain $T_H = 196$ MeV, $A = 0.5$ GeV$^{3/2}$, $M = 12$ GeV, and $B = (340$ MeV$)^4$. The fit for the trace anomaly Θ/T^4 is shown in Fig. 1. We also show the fit for the entropy density in Fig. 2. Both fits are within the error of lattice and mimic the behavior of the lattice results. As discussed in Ref. [13], a hadron resonance gas model with Hagedorn states uniquely fits the lattice data, whereas a hadron resonance gas without Hagedorn states completely misses the behavior.

BMW calculates the thermodynamical properties separately and, therefore, we fit only the energy density as

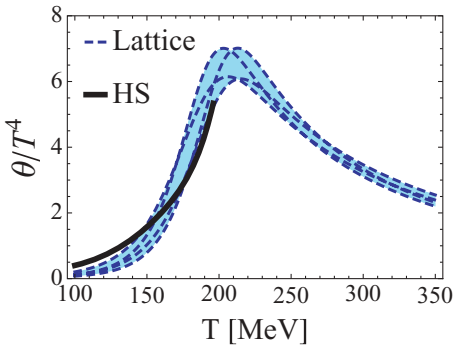

FIG. 1. (Color online) Comparison of trace anomaly to lattice QCD results from Refs. [18,19], where $T_c = 196$ MeV. HS is in reference to our model including Hagedorn states.

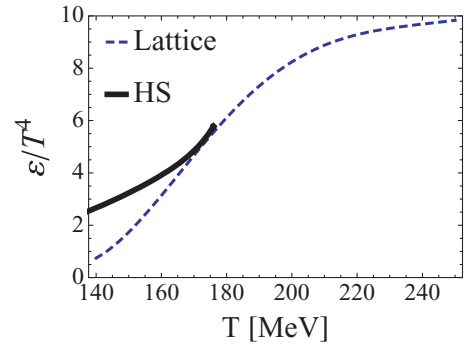

FIG. 3. (Color online) Comparison of energy density to lattice QCD results from Ref. [17], where $T_c = 176$ MeV. HS is in reference to our model including Hagedorn states.

shown in Fig. 3. From that we obtain $T_H = 176$ MeV, $A = 0.1$ GeV$^{3/2}$, $M = 12$ GeV, and $B = (300\ \text{MeV})^4$. We also show a comparison to the entropy density in Fig. 4. Our results with the inclusion of Hagedorn states are able to match lattice data near the critical temperature but do not match as well at lower temperatures in Figs. 1 and 2.

Our idea is that these very massive Hagedorn states exist, as pictured in Fig. 5, and are so large that they decay almost immediately into multiple pions and $X\bar{X}$ pairs. While it can be argued that Hagedorn states are more likely to decay into a pair of particles—a lighter Hagedorn state and another particle—these reactions are so quick that we can consider the end results, which would be multiple particles (mostly pions). That being said, it would be possible to put Hagedorn states into a transport approach such as UrQMD [28] using binary reactions with possible cross sections as described in Ref. [29]. We leave this as a challenge for the future.

Moreover, we need to consider the back reactions of multiple particles combining to form a Hagedorn state to preserve detailed balance. Rate equations provide us with a perfect tool for this because there are loss and gain terms that describe both the forward and the back reactions. Moreover, the state of chemical equilibrium is a fixed point of the rate equations. The rate equations for the Hagedorn resonances N_i, pions N_π, and the $X\bar{X}$ pair $N_{X\bar{X}}$, respectively, are given by

$$\begin{aligned}
\dot{N}_i &= \Gamma_{i,\pi}\left[N_i^{\text{eq}}\sum_n B_{i,n}\left(\frac{N_\pi}{N_\pi^{\text{eq}}}\right)^n - N_i\right] \\
&\quad + \Gamma_{i,X\bar{X}}\left[N_i^{\text{eq}}\left(\frac{N_\pi}{N_\pi^{\text{eq}}}\right)^{\langle n_{i,x}\rangle}\left(\frac{N_{X\bar{X}}}{N_{X\bar{X}}^{\text{eq}}}\right)^2 - N_i\right], \\
\dot{N}_\pi &= \sum_i \Gamma_{i,\pi}\left[N_i\langle n_i\rangle - N_i^{\text{eq}}\sum_n B_{i,n} n\left(\frac{N_\pi}{N_\pi^{\text{eq}}}\right)^n\right] \\
&\quad + \sum_i \Gamma_{i,X\bar{X}}\langle n_{i,x}\rangle\left[N_i - N_i^{\text{eq}}\left(\frac{N_\pi}{N_\pi^{\text{eq}}}\right)^{\langle n_{i,x}\rangle}\left(\frac{N_{X\bar{X}}}{N_{X\bar{X}}^{\text{eq}}}\right)^2\right], \\
\dot{N}_{X\bar{X}} &= \sum_i \Gamma_{i,X\bar{X}}\left[N_i - N_i^{\text{eq}}\left(\frac{N_\pi}{N_\pi^{\text{eq}}}\right)^{\langle n_{i,x}\rangle}\left(\frac{N_{X\bar{X}}}{N_{X\bar{X}}^{\text{eq}}}\right)^2\right]. \qquad (4)
\end{aligned}$$

The decay widths for the ith resonance are $\Gamma_{i,\pi}$ and $\Gamma_{i,X\bar{X}}$, the branching ratio is $B_{i,n}$ (see later in this article), and the average number of pions that each resonance will decay into is $\langle n_i\rangle$. The equilibrium values N^{eq} are both temperature- and chemical-potential-dependent. However, here we set $\mu_b = 0$. Equation (4) can also be rewritten in terms of fugacities (λ_i, λ_π, and $\lambda_{X\bar{X}}$), which are found by dividing each total number

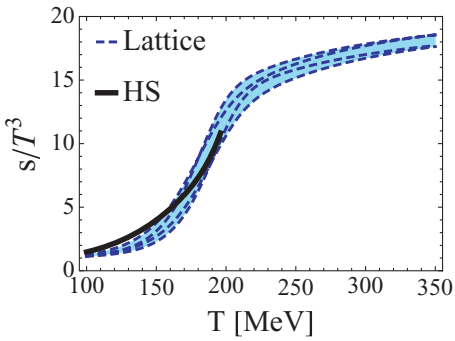

FIG. 2. (Color online) Comparison of entropy density to lattice QCD results from Refs. [18,19], where $T_c = 196$ MeV. HS is in reference to our model including Hagedorn states.

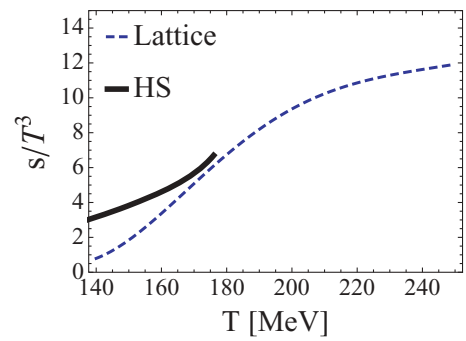

FIG. 4. (Color online) Comparison of entropy density to lattice QCD results from Ref. [17], where $T_c = 176$ MeV. HS is in reference to our model including Hagedorn states.

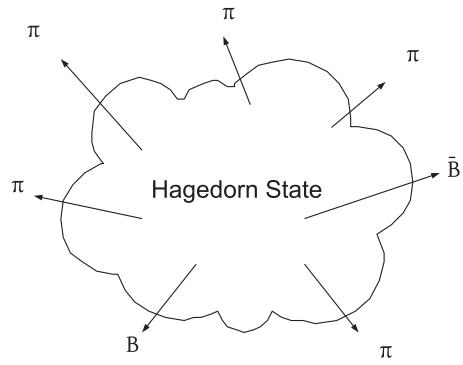

FIG. 5. Hagedorn states decay into multiple pions and an $X\bar{X}$ pair.

by its respective equilibrium value, for example, $\lambda_i = \frac{N_i}{N_i^{\rm eq}}$ (as seen for the baryon-antibaryon pairs in [11]). Additionally, a discrete spectrum of Hagedorn states is considered, which is separated into mass bins of 100 MeV. Each bin is described by its own rate equation.

The branching ratios, $B_{i,n}$, are the probability that the ith Hagedorn state will decay into n pions. Because we are dealing with probabilities, then $\sum_n B_{i,n} = 1$ must always hold. To include a distribution for our branching ratios, we assume that they follow a Gaussian distribution for the reaction HS $\leftrightarrow n\pi$

$$B_{i,n} \approx \frac{1}{\sigma_i\sqrt{2\pi}} e^{-\frac{(n-\langle n_i\rangle)^2}{2\sigma_i^2}}, \tag{5}$$

which has its peak centered at $\langle n_i\rangle$ and the width of the distribution is σ^2. Assuming a statistical, microcanonical branching for the decay of Hagedorn states, we can take a linear fit to the average number of pions in Fig. 1 in Ref. [10] (multiplying π^+ by three to include all pions) to find $\langle n_\pi\rangle$ such that $\langle n_i\rangle = 0.9 + 1.2\frac{m_i}{m_p}$ is the average pion number that each Hagedorn state decays into. Within the microcanonical model a Hagedorn state is defined by its mass and corresponding volume, where the volume is taken as $V = m_i/\varepsilon$. The mean energy density of a Hagedorn state is ε (taken as $\varepsilon = 0.5$ GeV/fm^3). Further discussions regarding this can be found in Refs. [10,30]. The width of the distribution is $\sigma_i^2 = (0.5\frac{m_i}{m_p})^2$, where m_p is the mass of the proton. Both of our choices in $\langle n_i\rangle$ and σ_i^2 roughly match the canonical description in Ref. [31].

Furthermore, we have the condition that each Hagedorn resonance must decay into at least two pions. Because of the nature of a Gaussian distribution, there is a nonzero probability that a Hagedorn state can decay into less than two pions. Therefore, we calculate the percentage of the distribution that falls below two pions and redistribute that over $n \geqslant 2$ so that $\sum_n B_{i,n} = 1$. This in turn leads to a new $\langle n_i\rangle$ and σ_i^2, which we find by calculating $\langle n_i\rangle = \sum_n nB_{i,n}$ and $\sigma_i^2 = \langle n_i^2\rangle - \langle n_i\rangle^2$. Thus, after we normalize for the cutoff $n \geqslant 2$, we have $\langle n_i\rangle \approx$ 3–34 and $\sigma_i^2 \approx 0.8$–510.

For the average number of pions when an $X\bar{X}$ pair is present, we again refer to the microcanonical model in Refs. [10,30]. We use $\langle n_\pi\rangle$ but then readjust it to the average pion number according to Fig. 2 in Ref. [10] for when a baryon-antibaryon pair is present (there the distribution is for a resonance of mass $m = 4$ GeV). Thus,

$$\langle n_{i,x}\rangle = \left(\frac{2.7}{1.9}\right)(0.3 + 0.4\,m_i) \approx 2\text{–}7, \tag{6}$$

where m_i is in GeV. In this article we do not consider a distribution but rather only the average number of pions when an $X\bar{X}$ pair is present. We assume that $\langle n_{i,x}\rangle = \langle n_{i,p}\rangle = \langle n_{i,k}\rangle = \langle n_{i,\Lambda}\rangle = \langle n_{i,\Omega}\rangle$ for when a proton antiproton pair, kaon antikaon pair, $\Lambda\bar{\Lambda}$, or $\Omega\bar{\Omega}$ pair is present. Ideally, $\langle n_{i,k}\rangle$, $\langle n_{i,\Lambda}\rangle$, and $\langle n_{i,\Omega}\rangle$ should be derived separately and will be done in a future presentation using a canonical model [32].

We used a linear fit for the total decay width similar to that used in Ref. [33]. The total decay width

$$\Gamma_i = 0.15\,m_i - 0.027 \tag{7}$$

(Γ_i and m_i in terms of GeV), which ranges from $\Gamma_i =$ 250 MeV to $\Gamma_i = 1800$ MeV, is a linear fit extrapolated from the data in Ref. [34]. However, in Eq. (4) the total decay width is separated into two parts: one for the reactions HS $\leftrightarrow n\pi$, $\Gamma_{i,\pi}$, and one for the reaction in Eq. (1), $\Gamma_{i,X\bar{X}}$, whereby $\Gamma_i = \Gamma_{i,\pi} + \Gamma_{i,X\bar{X}}$. Then relative decay width $\Gamma_{i,X\bar{X}}$ is the average number of $X\bar{X}$ in the system $\langle X\rangle$ multiplied by the total decay width Γ_i. Essentially, a fraction of the decay of the ith Hagedorn state goes into $X\bar{X}$ (set by the number of $X\bar{X}$ the ith Hagedorn state on average decays into) and the remainder goes into pions.

We find $\langle p\rangle$ by linearly fitting the proton in Fig. 2 in Ref. [10] so that

$$p = 0.058\,m_i - 0.10, \tag{8}$$

where m_i is in GeV and $\langle p\rangle \approx 0.01$–0.6. Thus, $\Gamma_{i,p\bar{p}}$ is between 3 and 1000 MeV. Clearly, $\Gamma_{i,\pi}$ is then $\Gamma_{i,\pi} = \Gamma_i - \langle p\rangle\Gamma_{i,\pi}$. Analogously for the kaons, the decay width is $\Gamma_{i,K\bar{K}} = \langle K\rangle\Gamma_i$, where

$$K^+ = 0.075\,m_i + 0.047, \tag{9}$$

where m_i is in GeV, which is also taken from Fig. 2 in Ref. [10]. We find that $\langle K\rangle = 0.2$ to 0.95 [10,30]. Thus, $\Gamma_{i,K\bar{K}}$ is between 50 and 1700 MeV.

For Λ we use a canonical model assuming that the baryon number $B = 0$, the strangeness $S = 0$, and the electrical charge $Q = 0$ to calculate the average Λ number. The results of this are shown in Fig. 6. We find that our $\langle\Lambda\rangle$ is lower than that from the microcanonical ensemble in [10], which is also shown in Fig. 6. This corresponds to a decay width of $\Gamma_{i,\Lambda\bar{\Lambda}} =$ 3–250 MeV.

Furthermore, the average number of Ω's is also shown in Fig. 6 from our canonical model, again assuming that the baryon number $B = 0$, the strangeness $S = 0$, and the electrical charge $Q = 0$. In Fig. 6 we multiply $\langle\Omega\rangle$ to better view the results. The resulting decay width is $\Gamma_{i,\Omega\bar{\Omega}} = 0.01$–4 MeV.

The equilibrium values are found using a statistical model [35], which includes 104 particles from the the PDG [34] (only light and strange particles). As in Ref. [35], we also consider the effects of feeding (the contributions of higher-lying resonances such as the ρ or ω resonances on the number of "pions" in our system; that is, $N_\pi^{\rm eq}$ includes "all" the pions from resonances from the PDG [34]). Feeding is also

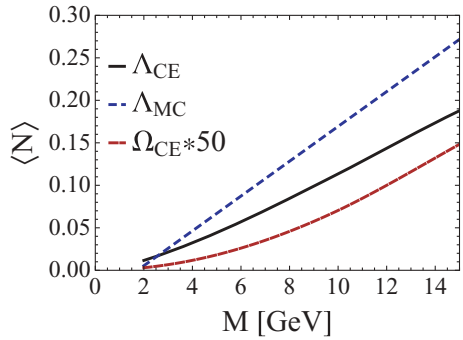

FIG. 6. (Color online) Average number of Λ's and Ω's. The Ω's are calculated within our canonical ensemble and the Λ's are calculated in both our canonical ensemble and a microcanonical ensemble.

considered for the protons, kaons, and Λ's. Additionally, throughout this article our initial conditions are the various fugacities at t_0 (at the point of the phase transition into the hadron gas phase),

$$\alpha \equiv \lambda_\pi(t_0), \quad \beta_i \equiv \lambda_i(t_0), \quad \text{and} \quad \phi \equiv \lambda_{X\bar{X}}(t_0), \tag{10}$$

which are chosen by holding the contribution to the total entropy from the Hagedorn states and pions constant; that is,

$$\begin{aligned} &s_{\text{Had}}(T_0,\alpha)V(t_0) + s_{\text{HS}}(T_0,\beta_i)V(t_0) \\ &\quad = s_{\text{Had+HS}}(T_0)V(t_0) = \text{const.} \end{aligned} \tag{11}$$

and the corresponding initial condition configurations we choose later can be seen later in this article in Table II. $s_{\text{Had}}(T_0,\alpha)$ is the entropy density at the initial temperature, that is, the critical temperature multiplied by our choice in α. Because the hadron resonance is dominated by pions, we can assume that α represents the initial fraction of pions in equilibrium. $s_{\text{HS}}(T_0,\beta_i)$ represents the entropy contribution from the Hagedorn states at T_c multiplied by the initial fraction of Hagedorn states in equilibrium. We hold α as a constant and then find the appropriate β_i. The volume expansion $V(t)$ is discussed in detail following Sec. V.

III. CHEMICAL EQUILIBRATION TIME ESTIMATE

As a starting point of our analysis, we first estimate the chemical equilibration time of the $X\bar{X}$ by looking at the fugacity of the $X\bar{X}$ rate equation; that is, Eq. (4) can be rewritten in terms of λ as shown for $B\bar{B}$ in Eq. (3) in Ref. [11], when both the pions and Hagedorn states are held constant. The $X\bar{X}$ rate equation then becomes

$$\dot{\lambda}_{X\bar{X}} = \sum_i \Gamma_{i,X\bar{X}} \frac{N_i^{\text{eq}}}{N_{X\bar{X}}^{\text{eq}}} \left(\beta_i - \alpha^{\langle n_{i,x}\rangle}\lambda_{X\bar{X}}^2\right), \tag{12}$$

which we can integrate,

$$\lambda_{X\bar{X}} = \zeta \left[\frac{\left(\frac{\phi+\zeta}{\phi-\zeta}\right) e^{\frac{2t}{\tau_{X\bar{X}}}} + 1}{\left(\frac{\phi+\zeta}{\phi-\zeta}\right) e^{\frac{2t}{\tau_{X\bar{X}}}} - 1} \right], \tag{13}$$

where

$$\begin{aligned} \tau_{X\bar{X}} &\equiv \frac{N_{X\bar{X}}^{\text{eq}}}{\sqrt{\sum_i \Gamma_{i,X\bar{X}} N_i^{\text{eq}} \beta_i}\sqrt{\sum_i \Gamma_{i,X\bar{X}} N_i^{\text{eq}} \alpha^{\langle n_{i,x}\rangle}}}, \\ \zeta &\equiv \sqrt{\frac{\sum_i \Gamma_{i,X\bar{X}} N_i^{\text{eq}} \beta_i}{\sum_i \Gamma_{i,X\bar{X}} N_i^{\text{eq}} \alpha^{\langle n_{i,x}\rangle}}}, \end{aligned} \tag{14}$$

and $\lambda_{X\bar{X}}(0) \equiv \phi$. Substituting in $\alpha = 1$ and $\beta_i = 1$ when the pions and Hagedorn states are in chemical equilibrium, we rederive Eq. (7) in Ref. [11],

$$\tau_{X\bar{X}} = \frac{N_{X\bar{X}}^{\text{eq}}}{\sum_i \Gamma_{i,X\bar{X}} N_i^{\text{eq}}}, \tag{15}$$

which is shown in Fig. 7. From Eq. (15) we see that the time scale has an indirect dependence on the decay width. Because the decay width has a linear dependence on the mass, the time scale decreases when more Hagedorn states are included. However, N_i^{eq} also decreases with increasing mass so above a certain point very many Hagedorn states need to be included to see an effect in the time scale. Furthermore, the chemical equilibrium values have a dependence on the temperature, which makes the time scale shortest for the highest temperatures.

In Figs. 8 and 9 we hold the Hagedorn states and pions and let the $X\bar{X}$ pairs reach chemical equilibrium. That means that in Eq. (4) we set $N_\pi = N_\pi^{\text{eq}}$ and $N_i = N_i^{\text{eq}}$ in the $\dot{N}_{X\bar{X}}$ equation. Figure 8 shows the results for $p\bar{p}$, $K\bar{K}$, and $\Lambda\bar{\Lambda}$, respectively, for $T_H = 176$ MeV and Fig. 9 shows the same

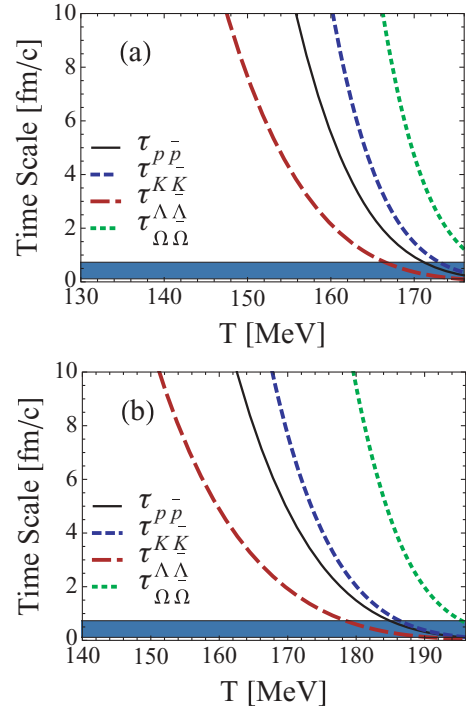

FIG. 7. (Color online) Comparison of the chemical equilibrium times for p's, K's, Λ's, and Ω's when $\alpha = 1$ and $\beta_i = 1$, where (a) $T_H = 176$ MeV and (b) $T_H = 196$ MeV. The band at the bottom of the panel is the range of chemical equilibrium times for the Hagedorn states (see Table I).

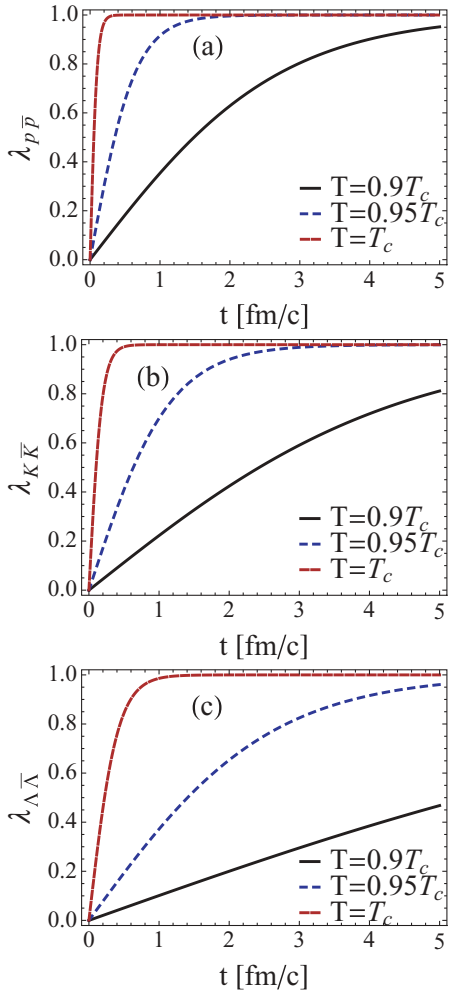

FIG. 8. (Color online) Graph of the number of proton-antiproton pairs, kaon-antikaon pairs, and Λ-anti-Λ pairs when both the resonances and the pions are held in equilibrium for $T_H = 176$ MeV.

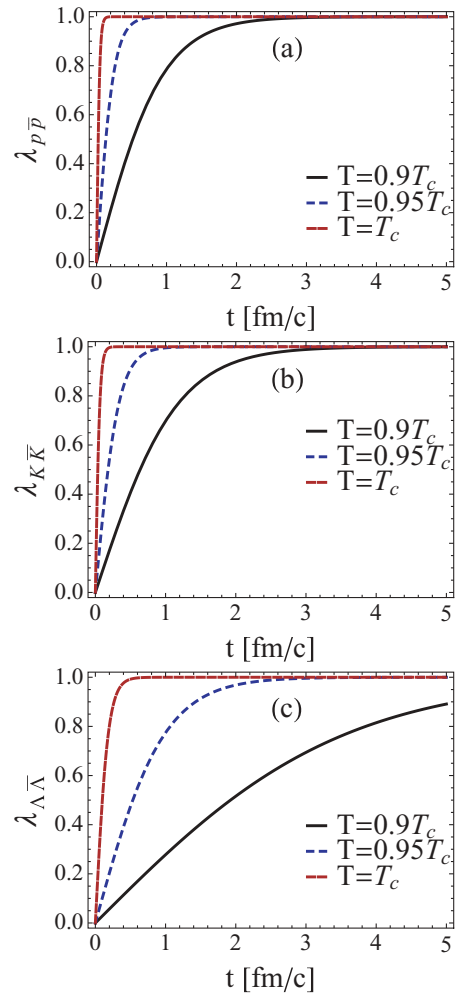

FIG. 9. (Color online) Graph of the number of proton-antiproton pairs, kaon-antikaon pairs, and Λ-anti-Λ when both the resonances and the pions are held in equilibrium for $T_H = 196$ MeV.

for $T_H = 196$ MeV. In all cases the temperature is held constant while the rate equations are solved over time. At $T = T_c$ all $X\bar{X}$ reach chemical equilibrium almost immediately (on the order of $t < 0.2$ fm/c). As T is decreased, the chemical equilibrium time obviously increases, which is clear from Fig. 7.

Even as the temperature is lowered we still see quick chemical equilibrium times. For the $p\bar{p}$ and $\Lambda\bar{\Lambda}$ pairs at $T = 0.9\,T_c$, the chemical equilibrium time is still about $t < 1$ fm/c. The $K\bar{K}$ pairs do have a slower chemical equilibrium time owing to their larger chemical equilibrium abundances, which is directly related to the chemical equilibration time through Eq. (4). This again represents the main idea, which is the importance of potential Hagedorn states in understanding fast chemical equilibration of hadrons close to and below T_c. The Hagedorn states increase dramatically in number close to the critical temperature and, thus, by its subsequent decay and repopulation they will quickly produce the various hadronic particles.

The equilibration of $X\bar{X}$ pairs then shown in Figs. 8 and 9, where the analytical result in Eq. (13) matches the numerical result exactly. From Figs. 8 and 9 it can be seen that all $X\bar{X}$ pairs equilibrate quickly close to the critical temperature $\tau < 1$ fm/c. Clearly, though, as the temperature decreases, the chemical equilibration time lengthens. However, at $T_H = 196$ MeV chemical equilibrium is still reached quickly, $\tau < 1$ fm/c.

IV. ANALYTICAL RESULTS: PIONS AND HAGEDORN RESONANCES

While the chemical equilibration time derived in the previous section is a good estimate, it can only be strictly applied when the pions and Hagedorn states are assumed to stay in chemical equilibrium at a constant temperature (Figs. 8 and 9). Otherwise, nonlinear effects that appear when the pions and Hagedorn states are allowed to equilibrate appear.

To understand the dynamics in more detail, we consider the simplified case when the Hagedorn resonances decay only into

TABLE I. Chemical equilibration times from analytical estimates where QE is quasiequilibrium at 95% of each respective T_H. Here $T_c^B = 176$ MeV and $T_c^B = 196$ MeV.

HS	$\tau_i = 1/\Gamma_i$	$M_{2\,\mathrm{GeV}}$ $0.8\,(\mathrm{fm}/c)$	$M_{12\,\mathrm{GeV}}$ $0.1(\mathrm{fm}/c)$
		$0.95T_c^B$	$0.95T_c^R$
$\lambda_\pi \approx 0$	$\tau_\pi^0 \equiv \dfrac{N_\pi^{\mathrm{eq}}}{\sum_i \Gamma_i N_i^{\mathrm{eq}} \langle n_i \rangle \beta_i}$	0.5	0.1
$\lambda_\pi \approx 1$	$\tau_\pi \equiv \dfrac{N_\pi^{\mathrm{eq}}}{\sum_i \Gamma_i N_i^{\mathrm{eq}} \langle n_i^2 \rangle}$	0.01	0.003
QE	$\tau_\pi^{\mathrm{QE}} \equiv \dfrac{N_\pi^{\mathrm{eq}}}{\sum_i \Gamma_i N_i^{\mathrm{eq}} \sigma_i^2} + \dfrac{\sum_{\mathrm{QE}} N_i^{\mathrm{eq}} \langle n_i^2 \rangle}{\sum_i \Gamma_i N_i^{\mathrm{eq}} \sigma_i^2}$	1.7	1.6

pions HS $\leftrightarrow n\pi$, which gives

$$\dot{N}_i = \Gamma_i \left[N_i^{\mathrm{eq}} \sum_{n=2} B_{i,n} \left(\frac{N_\pi}{N_\pi^{\mathrm{eq}}} \right)^n - N_i \right],$$
$$\dot{N}_\pi = \sum_i \Gamma_i \left[N_i \langle n_i \rangle - N_i^{\mathrm{eq}} \sum_{n=2} B_{i,n} n \left(\frac{N_\pi}{N_\pi^{\mathrm{eq}}} \right)^n \right]. \tag{16}$$

Assuming that the pions and the Hagedorn states described in Eq. (16) are then allowed to equilibrate near T_c in a static system, we are able to derive analytical solutions, the derivation of which is shown in detail in the Appendix . For the analytical solutions we divide the chemical equilibration into three stages, the chemical equilibration times of which are shown in Table I. The first stage (described by τ_π^0 in Table I) of the evolution is dominated by the chemical equilibration of the pions when the pions are still far away from their chemical equilibrium values. After the pions are close to chemical equilibrium, new dynamics take over, which are described by τ_π in Table I and Fig. 10.

In both Stage 1 and Stage 2 the equilibration of the Hagedorn states is set by the dynamics of the pions. Finally, in Stage 3 the pions, which are already almost in chemical equilibrium, reach a quasiequilibrium state with the Hagedorn states. Quasiequilibrium is reached when at least one species of Hagedorn states has succeeded its chemical equilibrium time scale determined from the inverse of its decay width, that is, $\tau_i = 1/\Gamma_i$. Because the heaviest Hagedorn states have the shortest τ_i's, then quasiequilibrium is reached when τ_i of the heaviest Hagedorn state is surpassed. During this stage nonlinear affects take over and, thus, a longer time scale, τ_π^{QE}, is seen. While this time scale may appear long, both the pions and the Hagedorn states are so close to chemical equilibrium that they are within roughly 10% (depending on the initial conditions) or less of their chemical equilibrium values before quasiequilibrium is even reached. The detailed calculations are shown in the Appendix.

Therefore, the most important chemical equilibration time is then that from the pions in Stage 1, that is, τ_π^0. The time scale from Stage 2 is so short that it is not of much importance. Additionally, by the time that Stage 3 is reached, both the pions and the Hagedorn states are essentially in chemical equilibrium

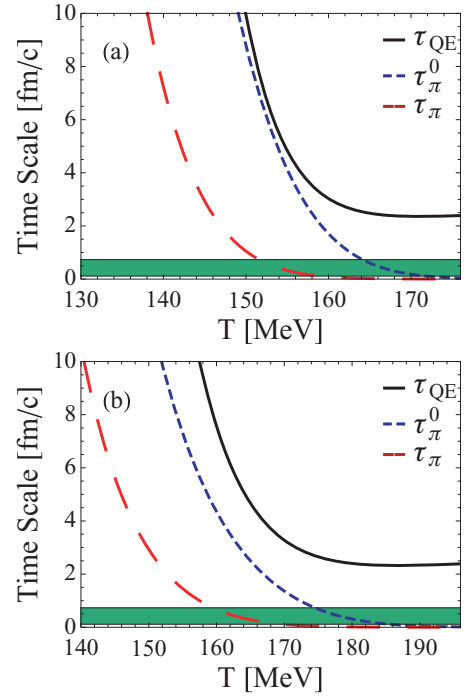

FIG. 10. (Color online) Comparison of the chemical equilibration times of the pions to the total chemical equilibration time for (a) $T_H = 176$ MeV and (b) $T_H = 196$ MeV.

and, therefore, the nonlinear affects do not play a large role in the overall chemical equilibration time. One can see this more clearly in Fig. 31(a) in the Appendix, where the pions and heavier Hagedorn states are extremely close to chemical equilibrium, while the lighter Hagedorn states are still only moderately close to their chemical equilibrium values. Therefore, the Hagedorn states and pions are able to be roughly in chemical equilibrium on the order of <1 fm/c, according to our analytical solution when held at a constant temperature.

This also applies to the $K\bar{K}$ reaction HS $\leftrightarrow n\pi + K\bar{K}$, as shown in Fig. 31(b) in the Appendix . The time scale for the pions and Hagedorn states are slightly longer when the $K\bar{K}$ pairs are present. The same goes for the estimated chemical equilibration time of the $K\bar{K}$ pairs in the previous section, $\tau_{K\bar{K}}$.

V. EXPANDING FIREBALL

To include the cooling of the fireball, we need to find a relationship between the temperature and the time, that is, $T(t)$. To do this, we apply a Bjorken expansion for which the total entropy is held constant

$$\mathrm{const} = s(T)V(t) \sim \frac{S_\pi}{N_\pi} \int \frac{dN_\pi}{dy} dy, \tag{17}$$

where $s(T)$ is the entropy density of the hadron gas with volume corrections.

The total number of pions in the 5% most central collisions, $\frac{dN_\pi}{dy}$, can be found from experimental results in Ref. [36]. There they found the phase-space yields for the pions π^+ (292.0) and π^- (290.9) using a Gaussian fit for yields as a function of the rapidity $\frac{dN_\pi}{dy}$, where we used the rapidity range $y = \pm 0.5$.

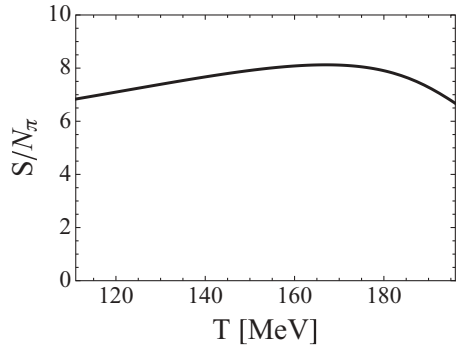

FIG. 11. Entropy per pion for a hadron gas in chemical equilibrium within the fireball ansatz.

We then assumed that the number of π^0's were also in that same range and took the average of the two to find 291.5. Thus, our total pion number is $\sum_i N_{\pi^i} = \int_{-0.5}^{0.5} \frac{dN_\pi}{dy} dy = 874$. While for a gas of noninteracting Bose gas of massless pions $S_\pi/N_\pi = 3.6$ we do have a mass for our pions, so we must adjust S_π/N_π accordingly. In Ref. [37] it was shown that when the pions have a mass the ratio changes and, therefore, the entropy per pion is close to $S_\pi/N_\pi \approx 5.5$. The actual S_π/N_π in our model is shown in Fig. 11 where $S_\pi/N_\pi \approx 6$, which is only slightly higher.

The effective volume at midrapidity can be parametrized as a function of time. We do this by using a Bjorken expansion and including accelerating radial flow. The volume term is then

$$V(t) = \pi\ ct\left[r_0 + v_0(t-t_0) + \tfrac{1}{2}a_0(t-t_0)^2\right]^2, \qquad (18)$$

where the initial radius is $r_0(t_0) = 7.1$ fm for $T_H = 196$ and the corresponding $t_0^{(196)} \approx 2$ fm/c. For $T_H = 176$ we allow for a longer expansion before the hadron gas phase is reached and, thus, calculate the appropriate $t_0^{(176)}$ from the expansion starting at $T_H = 196$, which is $t_0^{(176)} \approx 4$ fm/c (there is a slight variation dependence on the choice of v_0 and a_0). The $T(t)$

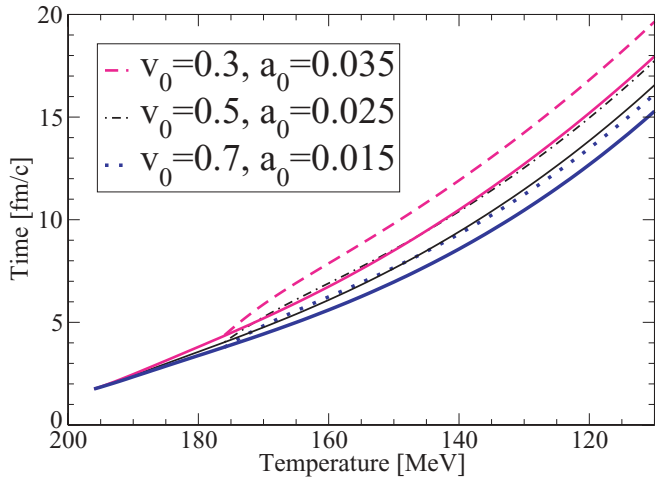

FIG. 12. (Color online) The temperature-time relationship is directly linked to the average transversel velocity chosen in Eq. (18) within the fireball model ansatz.

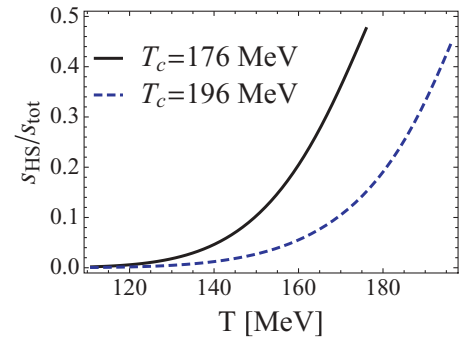

FIG. 13. (Color online) Ratio of the entropy of the Hagedorn states to the total entropy.

relation is shown in Fig. 12, which has almost no effect on the results as seen later in Fig. 16 and Fig. 17. Therefore, we choose $v_0 = 0.5$ and $a_0 = 0.025$ for the remainder of this article. The relation depicted allows to translate the later shown figures labeled by the effective global temperature of the evolving system directly into the evolving system time.

Because the volume expansion depends on the entropy according to Eq. (17) and the Hagedorn resonances contribute strongly to the entropy only close to the critical temperature (see Fig. 13), the equilibrium values actually decrease with increasing temperature close to T_c for the hadrons as seen in Figs. 14 and 15. One can clearly see from Fig. 13 that the Hagedorn states contribute strongly close to T_c down to about 80% of T_c.

Therefore, one has to include the potential contribution of the Hagedorn resonances to the pions as in the case of standard hadronic resonances, for example, a ρ meson decays dominantly into two pions and thus accounts for them by a factor two. This is similar to what was done in the Appendix in Eq. (A7). Including the Hagedorn-state contribution, we

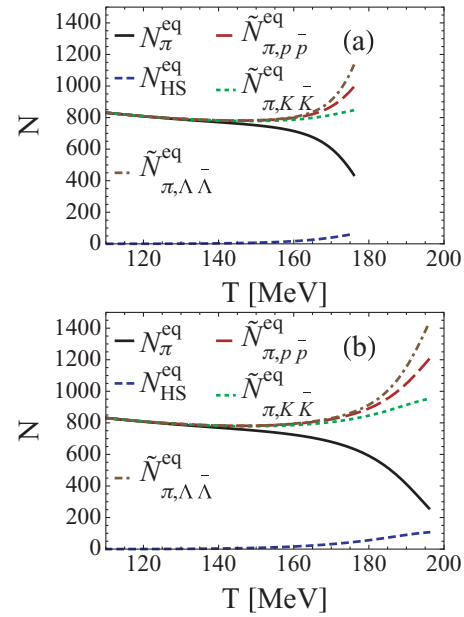

FIG. 14. (Color online) Comparison of the effective pion numbers when (a) $T_H = 176$ MeV or (b) $T_H = 196$ MeV.

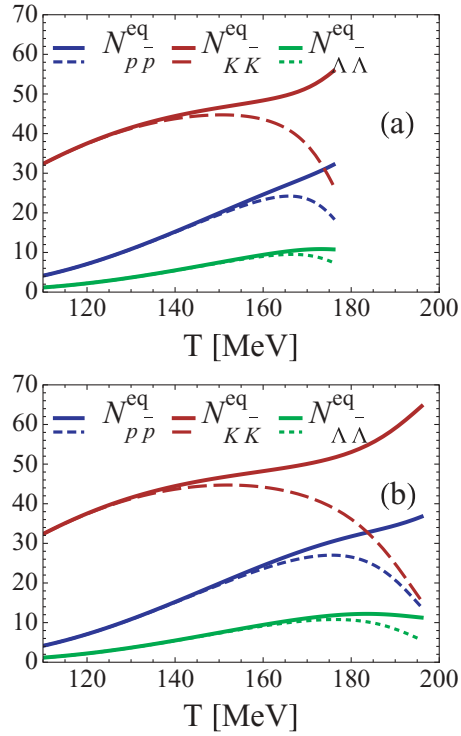

FIG. 15. (Color online) Comparison of the total number of $X\bar{X}$ and their effective numbers when (a) $T_H = 176$ MeV or (b) $T_H = 196$ MeV.

arrive at our effective number of pions

$$\tilde{N}_{\pi,X\bar{X}} = N_\pi + \sum_i N_i[(1 - \langle X_i\rangle)\langle n_i\rangle + \langle X_i\rangle\langle n_{i,x}\rangle], \quad (19)$$

which are shown in Fig. 14. In Fig. 14 we see that after the inclusion of the effective pion numbers the number of pions only decreases with decreasing temperature. Furthermore, in Fig. 14 the total number of Hagedorn states, $\sum_i N_i^{eq}$ is also shown. While there are by far fewer Hagedorn states present than pions, we see that they are important because of their large contribution to the entropy density, as shown in Fig. 13. The reason that the effective number of pions increases close to T_c is that the number of pions that the heavy Hagedorn states decay into is large. If $\langle n_i\rangle$ was smaller or no longer linear, it could be possible that the effective number of pions would remain constant.

Moreover, it is useful to consider the effective number of $X\bar{X}$ pairs

$$\tilde{N}_{X\bar{X}} = N_{X\bar{X}} + \sum_i N_i\langle X_i\rangle \quad (20)$$

because Hagedorn states also contribute strongly to the $X\bar{X}$ pairs close to T_c, as seen in Fig. 15. Again we see that only the effective number of $X\bar{X}$ pairs have consistent decreasing behavior with decreasing temperature, whereas without the Hagedorn-state contributions we see a decrease close to T_c.

TABLE II. Initial condition configurations, recalling Eq. (10).

	$\alpha = \lambda_\pi(t_0)$	$\beta_i = \lambda_i(t_0)$	$\phi = \lambda_{X\bar{X}}(t_0)$
IC_1	1	1	0
IC_2	1	1	0.5
IC_3	1.1	0.5	0
IC_4	0.95	1.2	0

Along with the expansion, we also must solve these rate equations [Eq. (4)] numerically.[1] We start with various initial conditions, as mentioned previously, that are described by α, β_i, and ϕ (see Table II). The initial temperature is the respective critical temperature and we end the expansion at $T = 110$ MeV, a global kinetic freezeout temperature.

For the remainder of this article we include only results for an expanding fireball, which are solved numerically. As an initial test we hold both the pions and the Hagedorn states in chemical equilibrium and allow just $X\bar{X}$ to equilibrate, as seen in Figs. 16 and 17. The black solid line in each graph is the chemical equilibrium abundances and the colored lines are the dynamical calculations for various expansions that follow the $T(t)$ shown in Fig. 12. We see that regardless of our volume expansion they all quickly approach equilibrium. In Figs. 16 and 17 the $X\bar{X}$ all reach chemical equilibrium almost immediately, well before $0.9T_c$ the chemical equilibration time is <1 fm/c. The only exception is the $K\bar{K}$ pairs for $T_H = 176$ MeV. However, we see later on that the K/π ratio matches the data.

More interestingly, we consider the case when the pions, Hagedorn states, and $X\bar{X}$ all are allowed to chemical equilibrate. We then vary the initial conditions and observe their effects. The results for $p\bar{p}$ pairs are shown in Figs. 18 and 19. In Figs. 18 and 19 we show the evolution of both the $p\bar{p}$ pairs and the pions for the reaction $n\pi \leftrightarrow \text{HS} \leftrightarrow n\pi + X\bar{X}$. Note that in all the following figures the effective numbers are shown so that the contribution of the Hagedorn states is included.

One can see that the chemical equilibration time does depend slightly on our choice of β_i; that is, a larger β_i means a quicker chemical equilibration time. For instance, if the Hagedorn states were overpopulated coming out of the QGP phase, then chemical equilibrium times would be slightly shorter. However, even when the Hagedorn resonances start underpopulated, the $p\bar{p}$ pairs are able to reach chemical equilibrium immediately. Additionally, when the $p\bar{p}$ pairs start at about half their chemical equilibrium values, it only helps the $p\bar{p}$ pairs to reach equilibrium at a slightly higher temperature (on the order of a couple of MeV). Additionally, we see a greater dependence on β_i for $T_H = 176$ MeV than for $T_H = 176$ MeV. Throughout the evolution we see from the pions that they remain roughly in chemical equilibrium. Thus, our initial analytical approximation appears reasonable.

In Fig. 20, the ratio of protons to π's is shown. We also compare our results to that of experimental data. We see that

[1]We solve our coupled nonlinear differential equations using NDSOLVE in MATHEMATICA.

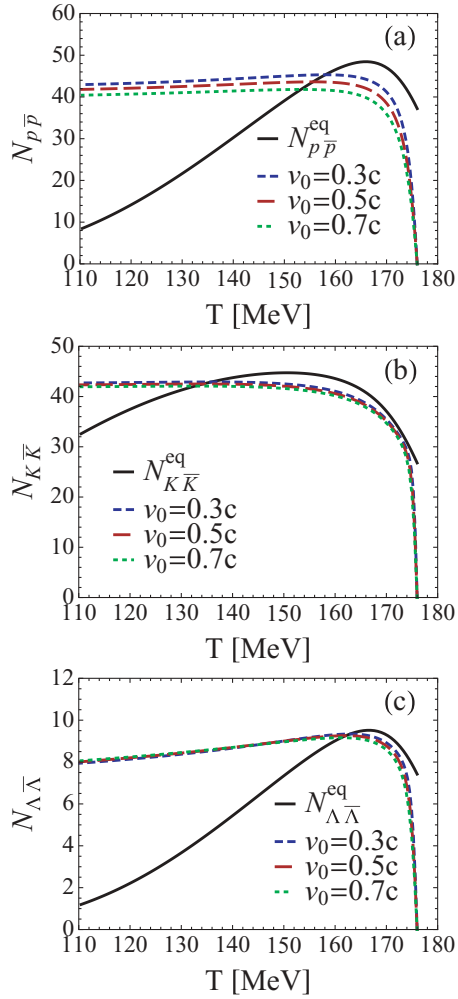

FIG. 16. (Color online) Results for the (a) $p\bar{p}$, (b) $K\bar{K}$, and (c) $\Lambda\bar{\Lambda}$ when the pions and Hagedorn resonances are held in equilibrium for $T_H = 176$ MeV.

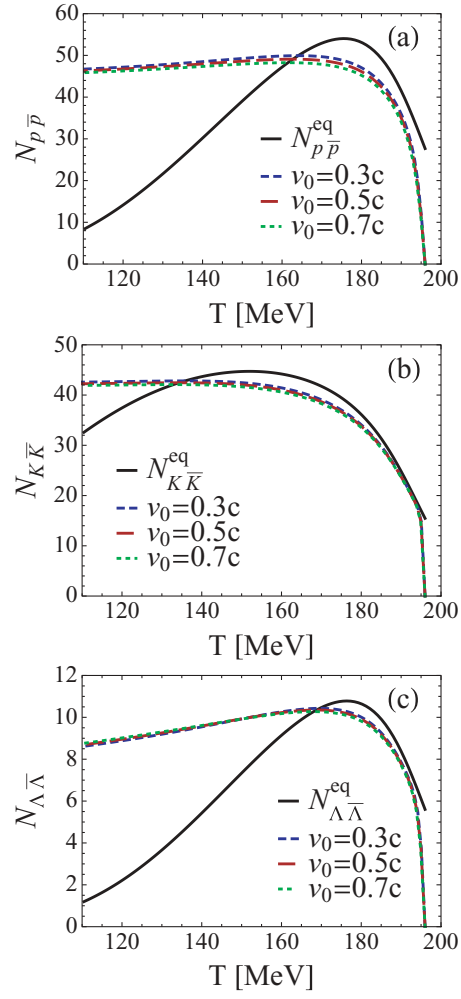

FIG. 17. (Color online) Results for the (a) $p\bar{p}$, (b) $K\bar{K}$, and (c) $\Lambda\bar{\Lambda}$ when the pions and Hagedorn resonances are held in equilibrium for $T_H = 196$ MeV.

for $T_H = 176$ MeV our results enter the band of experimental data before $T = 170$ MeV and remain there throughout the entire expansion regardless of the initial conditions. However, for $T_H = 176$ MeV the results are slightly different. In this case, the ratios match the experimental data early on at around $T = 190$ MeV. However, they become briefly overpopulated around $T = 160$–170 MeV but then quickly return to the experimental values, except for the case when we have initial conditions such that the pions are overpopulated. This could imply that there are a few too many Hagedorn states and a fit for the Hagedorn states with a lower A (degeneracy of the Hagedorn states) may produce better results.

As with the protons, the total number of kaons are also slightly dependent on our chosen initial conditions, more specifically, our choice in β_i. In Figs. 21 and 22 the temperature of the evolving system after the phase transition at which chemical equilibrium among standard hadrons is basically reached and maintained is between $T = 160$ and $T = 170$ for $T_H = 176$ MeV and they have also already reached chemical equilibrium by $T = 170$ for $T_H = 196$ MeV, below which the Hagedorn states basically die out. The one exception is when the Hagedorn states begin underpopulated, that is, when $\beta_i < 1$. In this case, the kaon pairs take longer to reach chemical equilibrium. However, when we look at K/π in Fig. 23, lower β_i actually fits the data better.

Moreover, the pions again remain roughly at chemical equilibrium throughout the expansion as seen in Figs. 21 and 22. While the pion graphs look roughly similar in Figs. 18–22, they are not. The difference is how the pions are affected in the presence of a $p\bar{p}$ pair compared to a decay that includes a kaon antikaon pair.

In Fig. 23 the ratio of kaons to pions is shown for $T_H = 176$ MeV and for $T_H = 196$ MeV. For $T_H = 176$ MeV our results are roughly at the upper edge of the experimental values. However, for $T_H = 196$ MeV our results are slightly higher than the experimental values, although the results at $T = 110$ MeV are almost exactly those of the uppermost experimental data point.

We can also observe the effects of the expansion on the $\Lambda\bar{\Lambda}$ pairs as seen in Figs. 24 and 25. We see that both reach the experimental values almost immediately ($T > 170$ for $T_H = 176$ MeV and around $T = 190$ for $T_H = 196$ MeV). The one

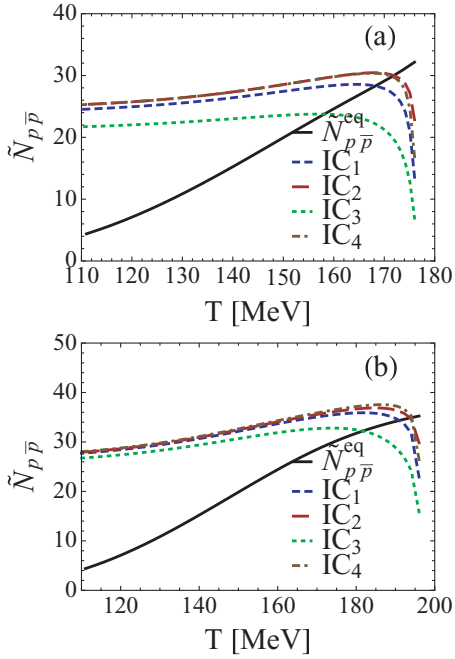

FIG. 18. (Color online) Results for the (a) p's and (b) pions with various initial conditions for $T_H = 176$ MeV.

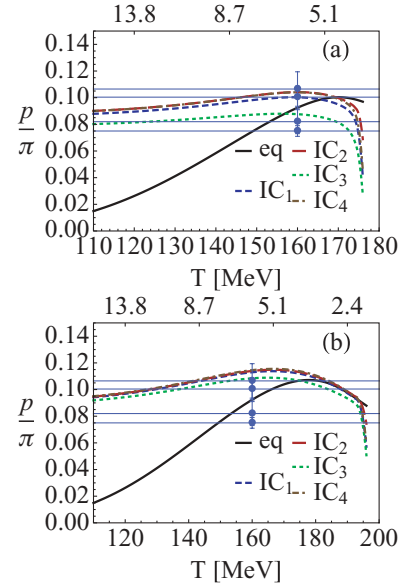

FIG. 20. (Color online) Results for the ratio of p's with various initial conditions for (a) $T_H = 176$ MeV or (b) $T_H = 196$ MeV. Note that for STAR $p/\pi^- = 0.11$ and $\bar{p}/\pi^- = 0.082$.

exception is again for an underpopulation of Hagedorn states, which reaches chemical equilibrium at $T \approx 165$ for $T_H = 176$ MeV and already by $T = 170$ for $T_H = 196$ MeV.

The ratio of Λ/π's is shown in Fig. 26. In both cases, the Λ/π's match the experimental values extremely well. For $T_H = 176$ MeV our results reach the equilibrium values at $T \approx 170$ MeV and for $T_H = 196$ MeV the experimental values are reached already by $T \approx 170$ MeV.

A summary graph of all our results is shown in Fig. 27. The black error bars cover the range of error for the experimental data points from both STAR and PHENIX. The points show the range in values for the various initial conditions at $T = 110$ MeV. We see in our graph that our freeze-out results match the experimental data well.

What the graphs in Figs. 18–26 show us is that a dynamical scenario is able to explain chemical equilibration values that appear in thermal fits by $T = 160$ MeV. In general, $T_H = 176$ MeV and $T_H = 196$ give chemical freeze-out values in

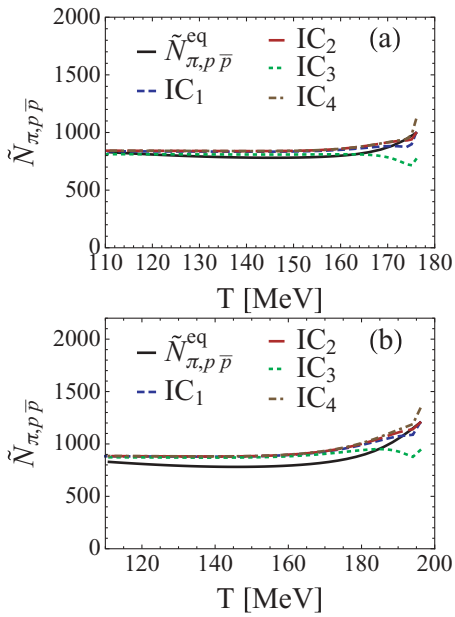

FIG. 19. (Color online) Results for the (a) p's and (b) pions with various initial conditions for $T_H = 196$ MeV.

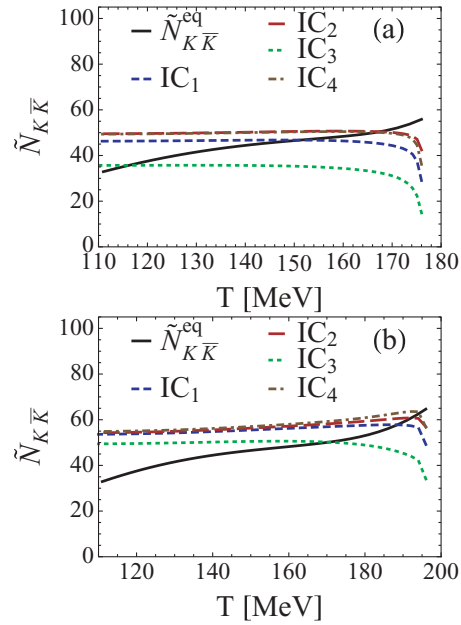

FIG. 21. (Color online) Results for the (a) K's and (b) pions with various initial conditions for $T_H = 176$ MeV.

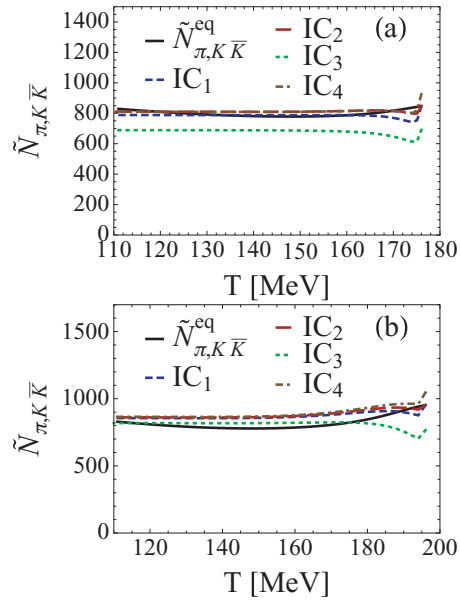

FIG. 22. (Color online) Results for the (a) K's and (b) pions with various initial conditions for $T_H = 196$ MeV.

the range between $T = 160$ and $T = 170$ MeV. These results agree well with the chemical freeze-out temperature found in Ref. [16].

Moreover, the initial conditions have little effect on the ratios and give a range in the chemical equilibrium temperature of about ∼5 MeV, which implies that information from the QGP regarding multiplicities is washed out owing to the rapid dynamics of Hagedorn states. Lower β_i does slow the chemical

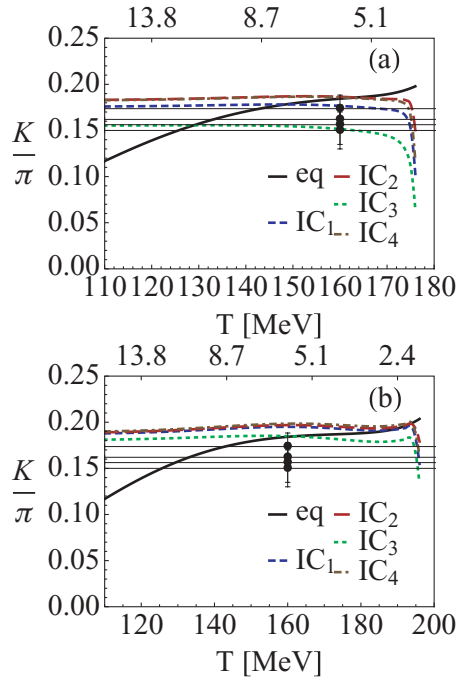

FIG. 23. (Color online) Results for the ratio of K's with various initial conditions for (a) $T_H = 176$ MeV or (b) $T_H = 196$ MeV. Note that for STAR $K^+/\pi^- = 0.16$ and $K^-/\pi^- = 0.15$.

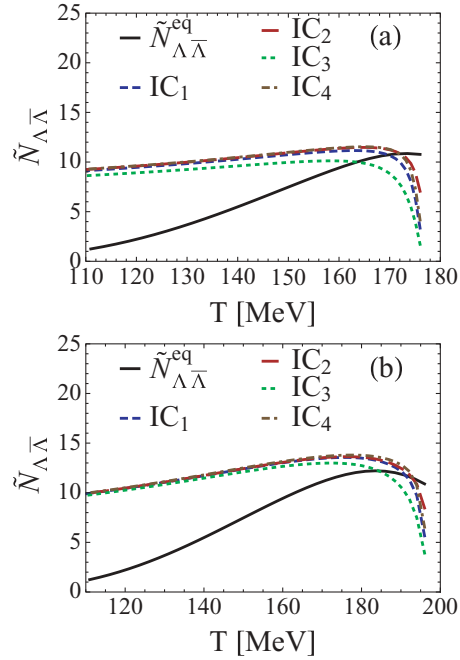

FIG. 24. (Color online) Results for the (a) Λ's and (b) pions with various initial conditions for $T_H = 176$ MeV.

equilibrium time slightly. However, as seen in Fig. 27 they still fit well within the experimental values. Furthermore, in Ref. [11] we showed that the initial condition plays pretty much no roll whatsoever in the ratios of K/π^+ and $(B + \bar{B})/\pi^+$, thus strengthening our argument that the dynamics are washed out following the QGP.

While the variance in the chemical equilibration time arising from the initial conditions may seem contradictory to the K/π^+ and $(B + \bar{B})/\pi^+$ ratios in Ref. [11], it can be explained with the pion populations. In Figs. 18–22, quicker

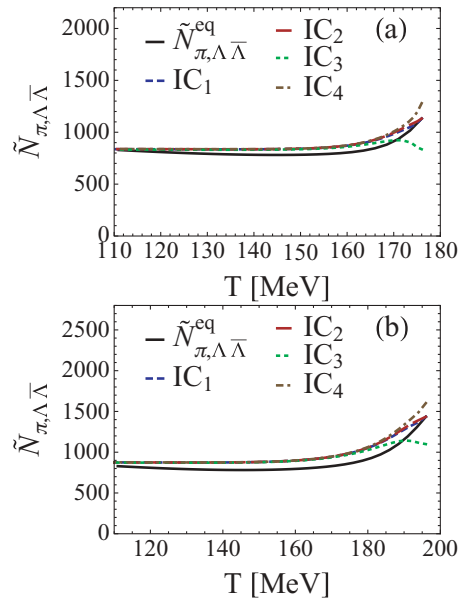

FIG. 25. (Color online) Results for the (a) Λ's and (b) pions with various initial conditions for $T_H = 196$ MeV.

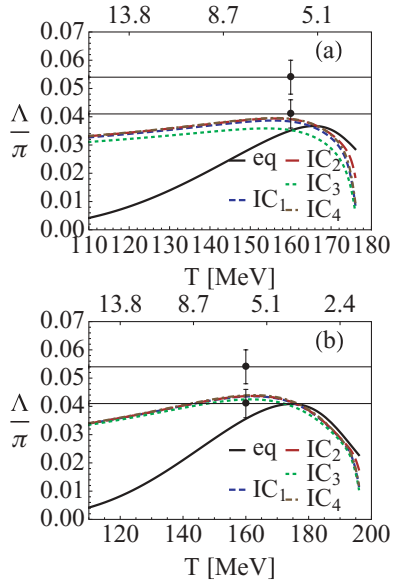

FIG. 26. (Color online) Results for the ratio of Λ/π's with various initial conditions for (a) $T_H = 176$ MeV or (b) $T_H = 196$ MeV. Note that for STAR $\Lambda/\pi^- = 0.54$ and $\bar{\Lambda}/\pi^- = 0.41$.

chemical equilibration times, and thus larger total baryon/kaon numbers, translated into a larger number of pions in the system. Thus, the K/π^+ and $(B + \bar{B})/\pi^+$ ratios do not depend on the initial conditions.

VI. PRODUCTION OF $\Omega\bar{\Omega}$

We can also use our model to investigate the possibility of Ω's. In Ref. [10], they discussed the possibility of Ω's being produced from the following decay channels:

$$\begin{aligned} \mathrm{HS} &\leftrightarrow \Omega\bar{\Omega} + X, \\ \mathrm{HS}\,(sss\bar{q}\bar{q}\bar{q}) &\leftrightarrow \Omega + \bar{B} + X, \\ \mathrm{HS}_B(sss) &\leftrightarrow \Omega + X. \end{aligned} \tag{21}$$

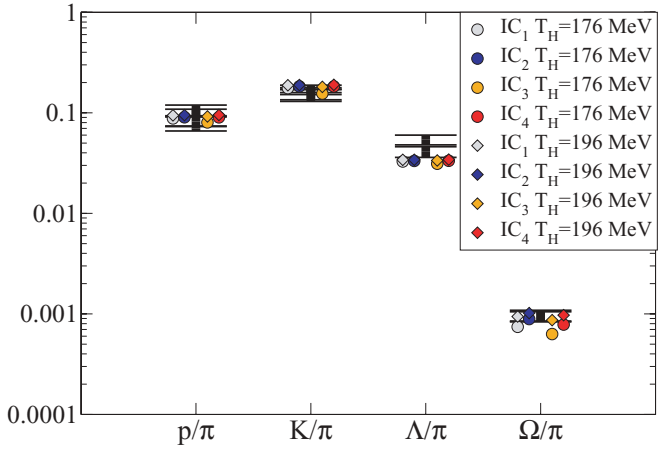

FIG. 27. (Color online) Plot of the various ratios including all initial conditions defined in Table II. The points show the ratios at $T = 110$ MeV for the various initial conditions (circles are for $T_H = 176$ MeV and diamonds are for $T_H = 196$ MeV). The experimental results for STAR and PHENIX are shown by the black error bars.

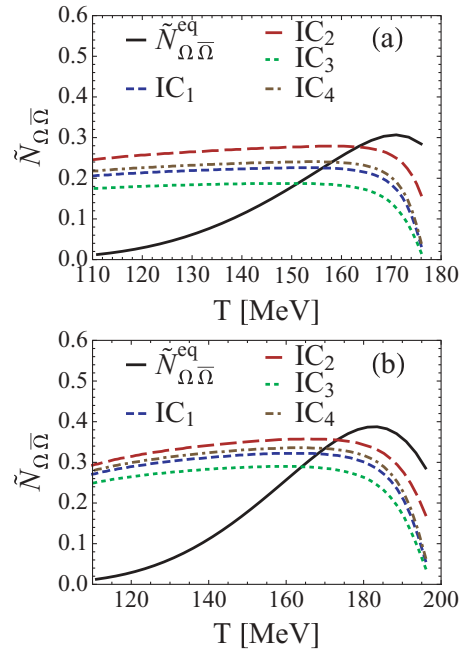

FIG. 28. (Color online) Results for the (a) Ω's and (b) pions with various initial conditions for $T_H = 176$ MeV.

The first decay channel of a mesonic nonstrange Hagedorn state we can implement straightforwardly with our model by employing the canonical branching ratio via Fig. 6. The results are shown in Fig. 28 for $T_H = 176$ MeV and in Fig. 29 for $T_H = 196$ MeV; the Ω/π ratio is shown in Fig. 30. We are able to find the average number of Ω's from Ref. [32], as seen in Fig. 6. We see that, using only the first reaction, we are still impressively able to adequately populate the $\Omega\bar{\Omega}$ pairs so that they roughly match the experimental data. However, from Fig. 7 we see that for the Ω particle, the equilibration

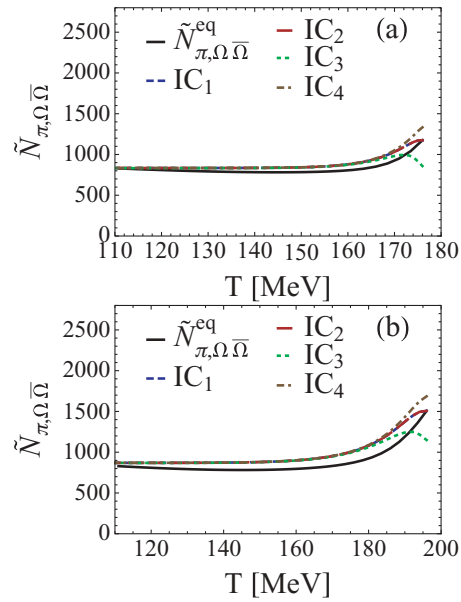

FIG. 29. (Color online) Results for the (a) Ω's and (b) pions with various initial conditions for $T_H = 196$ MeV.

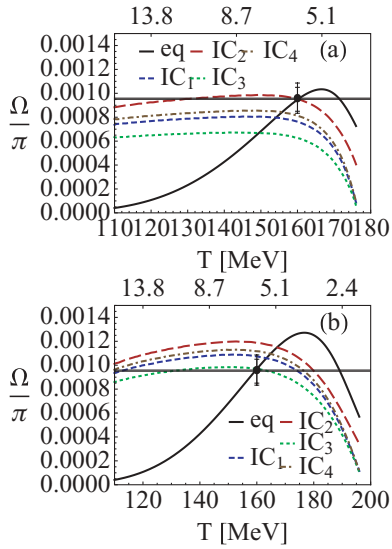

FIG. 30. (Color online) Results for the ratio of Ω/π's with various initial conditions for (a) $T_H = 176$ MeV or (b) $T_H = 196$ MeV. Note that for STAR $\Omega/\pi^- = 9.5 \times 10^{-4}$ and $\bar{\Omega}/\pi^- = 9.6 \times 10^{-4}$.

times are short only very close to T_c. The scenario is thus more delicate. If one would take, for example, one half or one fourth, respectively, of the decay width of that of Eq. (7), the total production of Ω is not sufficient up to 25% or 50%, respectively, to meet the experimental yield (the other ratios are not significantly affected by such a change of the decay width).

In a future work, it would be interesting to observe the other decay channels, as given in Eq. (21) and described in Ref. [10]. The second reaction includes a mesonic, three-times-strange Hagedorn state, whereas the third decay channel includes a baryonic, strange Hagedorn state. Both states are much more likely to directly decay into a Ω. These are, admittedly, exotic states, but should also occur in the spirit of Hagedorn states. To observe these decay channels, a method, for example, a microscopic quark model, must be found to find the appropriate Hagedorn spectrum for strange mesonic and baryonic Hagedorn states.

VII. CONCLUSIONS

In this article we found that hadronic matter, at RHIC or SPS energies, can reach chemical equilibrium within a dynamical scenario using Hagedorn states close to the critical temperature. These states were able to produce quick chemical equilibration times in (anti-)protons, (anti-)kaons, and (anti-)Λ's close to the critical temperature owing to their strong increase in their abundancy. The existence of such a mixture of standard hadrons and Hagedorn states just below the phase transition can explain dynamically the chemical equilibration of the hadronic species at around temperatures of 160 to 170 MeV, as seen within the thermal models.

From our analytical results we found that the chemical equilibration time depends on the temperature, decay widths, and branching ratios, but not the initial conditions. While this changes slightly when an expanding fireball is considered, the initial condition still only play a small role and only minimally affect the "freeze-out" temperature at which chemical equilibrium is reached. This demonstrates that regardless of the population of hadrons coming out of the QGP phase, the initial conditions are washed out and everything can reach abundances which correspond to those of chemical equilibrium by the chemical freeze-out temperatures found in Ref. [16].

Moreover, from our previous article [11], we showed that particle ratios $[K/\pi^+$ and $(B + \bar{B})/\pi^+]$ are not affected by the initial conditions and here we showed that p/π, K/π, Λ/π, and also Ω/π match the experimental values regardless of the initial conditions. Figure 27 demonstrates this especially nicely and summarizes our findings: Regardless of the initial conditions, our dynamical scenario can match experimental data. We do find, however, that $T_H = 196$ fits within the experimental data box for K/π, whereas $T_H = 176$ is slightly above. This appears to reconfirm the findings in Ref. [16].

Our results imply that both lattice temperature can ensure that the hadrons reach their chemical equilibrium values by $T = 160$–170 MeV. Although the ratios for $T_H = 176$ do fit the data somewhat better, both match the experimental values reasonably well. This implies that, independent of the critical temperature, the hadrons are able to reach chemical freeze-out.

We see sufficiently short time scales for the chemical equilibrium of hadrons. The protons, kaons, and Λ's reach chemical equilibrium on the order of $\Delta\tau \approx 1$–2 fm/c. Moreover, Hagedorn states provide a very efficient way for incorporating multihadronic interactions (with parton rearrangements).

In an upcoming presentation we will use a canonical model to derive all the branching ratios included in our calculations. We can then look at reactions that include a mixture of strange and nonstrange baryons (for instance, $\bar{p} + \Lambda$) and multistrange baryons. However, considering that our initial results produce quick chemical equilibration times for the baryons, kaons, and Λ's, it is reasonable to believe that this will occur for mixed reactions and multistrange baryons as well. In addition, the machinery of standard hadronic reactions, that is, binary scattering processes and resonance production processes, help also to equilibrate the various hadronic degrees of freedom. Still, our work indicates that the population and repopulation of potential Hagedorn states close to phase boundary can be the key source for a dynamical understanding of generating and chemically equilibrating the standard and measured hadrons.

ACKNOWLEDGMENTS

J.N.H. thanks J. Noronha, B. Cole, and M. Gyulassy for productive discussions. This work was supported by the Helmholtz International Center for FAIR within the framework of the LOEWE Program (Landes-Offensive zur Entwicklung Wissenschaftlich-ökonomischer Exzellenz) launched by the State of Hesse. I.A.S. thanks the members of the Institut für Theoretische Physik of Johann Wolfgang Goethe-Universität

for their hospitality during the final stages of this work. The work of I.A.S. was supported in part by the start-up funds from the Arizona State University.

APPENDIX: ANALYTICAL SOLUTIONS OF VARIOUS EQUILIBRATION PROCESSES

If our initial conditions are such that both the pions and the Hagedorn states begin far out of chemical equilibrium, we can find an analytical solution by subdividing the analysis into three distinct stages. Initially, during Stage 1 the pions are underpopulated such that we can say that they approximately begin at $\alpha \approx 0$ (we can also start the pions above zero, and the approximation works well). Because the pions reach chemical equilibrium much quicker than the Hagedorn states owing to all the Hagedorn states decaying quickly into pions, then we can make the approximation that the Hagedorn states are held at their initial value of β_i. One can see this from the difference in the time scales from Table I, where $\tau_i > \tau_\pi^0$ and $\tau_i > \tau_\pi$. Because $\alpha \approx 0$ we let $\lambda_\pi^n \approx 0$, then substituting this into Eq. (16) we obtain

$$\begin{aligned} \dot{\lambda}_\pi &= \sum \Gamma_i \frac{N_i^{\rm eq}}{N_\pi^{\rm eq}} \beta_i \langle n_i \rangle, \\ \lambda_\pi &= \left(\frac{t}{\tau_\pi^0} + \alpha \right), \end{aligned} \tag{A1}$$

which is the fugacity of the pions in Stage 1 and gives $\tau_\pi^0 \equiv \frac{N_\pi^{\rm eq}}{\sum_i \Gamma_i N_i^{\rm eq} \langle n_i \rangle \beta_i}$. Again, using the approximation $\alpha \approx 0$ and substituting Eq. (A1) into the Hagedorn-state rate equation in Eq. (16), with the solution

$$\begin{aligned} \dot{\lambda_i} &= \Gamma_i \left[\left(\frac{t}{\tau_\pi^0} \right)^{\langle n_i \rangle} - \lambda_i \right], \\ \lambda_i &= \left[1 - \langle n_i \rangle \left(\frac{-t}{\tau_i} \right)^{-\langle n_i \rangle} e^{-\left(\frac{t}{\tau_i}\right)} \int_0^{-\frac{t}{\tau_i}} x^{\langle n_i \rangle - 1} e^{-x} dx \right] \\ &\quad \times \left(\frac{t}{\tau_\pi^0} \right)^{\langle n_i \rangle} + \beta_i e^{-\left(\frac{t}{\tau_i}\right)}. \end{aligned} \tag{A2}$$

Substituting $x = \frac{t}{\tau_i}\xi$ into the integral in Eq. (A2), expanding the exponential inside the integral so $e^y = \sum_{j=0}^{\infty} \frac{y^j}{j!}$, and integrating over ξ provides us with the fugacity of the Hagedorn states in Stage 1:

$$\begin{aligned} \lambda_i &= \left(\frac{t}{\tau_\pi^0} \right)^{\langle n_i \rangle} \left[1 - e^{-\left(\frac{t}{\tau_i}\right)} \sum_{j=0}^{\infty} \frac{\langle n_i \rangle}{j!(\langle n_i \rangle + j)} \left(\frac{t}{\tau_i} \right)^j \right] \\ &\quad + \beta_i e^{-\left(\frac{t}{\tau_i}\right)}. \end{aligned} \tag{A3}$$

Therefore, Eqs. (A1) and (A3) describe the behavior of the pions and Hagedorn states during the initial stage of the evolution toward chemical equilibrium. They are then compared to the numerical results in Fig. 31.

As the pions near equilibrium, our approximation of $\lambda_\pi \approx 0$ no longer holds and we switch to Stage 2, where we assume $\lambda_\pi \approx 1$ at time t_1. Here t_1 is a time when the pions are almost in chemical equilibrium, which is normally taken when the pions reach about ~95% of their chemical equilibrium value. Returning to the pion equation in Eq. (16), we can substitute in $\lambda_\pi = 1 - \epsilon$ and use the approximation $(1-\epsilon)^n \approx 1 - n\epsilon$:

$$\dot{\epsilon} = -\sum \Gamma_i \frac{N_i^{\rm eq}}{N_\pi^{\rm eq}} \left[(\beta_i - 1)\langle n_i \rangle + \langle n_i^2 \rangle \epsilon \right]. \tag{A4}$$

Additionally, we substituted in β_i for λ_i as an approximation because the Hagedorn states do not change significantly in Stage 1 (the majority of the evolution is done by the pions). Recall that $\beta_i = \lambda_i(t = 0)$ and it is a constant. In its present form, Eq. (A4) can be integrated. We also define $\epsilon(t_1) = 1 - \eta$, where η is close to 1 (η is the measurement of how close the pions are to their equilibrium value when we switch from Stage 1 to Stage 2). Then, after integration,

$$\lambda_\pi = \left[1 + \gamma - (1 + \gamma - \eta) e^{-\frac{t - t_1}{\tau_\pi}} \right], \tag{A5}$$

where $\gamma = \frac{\sum_i \Gamma_i N_i^{\rm eq} (\beta_i - 1)\langle n_i \rangle}{\sum_i \Gamma_i N_i^{\rm eq} \langle n_i^2 \rangle}$ and $\tau_\pi \equiv \frac{N_\pi^{\rm eq}}{\sum_i \Gamma_i N_i^{\rm eq} \langle n_i^2 \rangle}$. Analogously to Stage 1, we substitute the pion equation, that is, Eq. (A5), into the Hagedorn resonance equation in Eq. (16) and integrate

$$\begin{aligned} \lambda_i &= \left[d e^{-\frac{t - t_1}{\tau_i}} + 1 + \langle n_i \rangle \gamma \right. \\ &\quad \left. - \left(\frac{\tau_\pi}{\tau_\pi - \tau_i} \right) \langle n_i \rangle (1 + \gamma - \eta) e^{-\frac{t - t_1}{\tau_\pi}} \right], \end{aligned} \tag{A6}$$

where $d = \omega_i - 1 + \langle n_i \rangle \gamma + (\frac{\tau_\pi}{\tau_\pi - \tau_i}) \langle n_i \rangle (1 + \gamma - \eta)$ and $\lambda_i(t_1) = \omega_i$. Thus, our equations for the evolution of the pions and Hagedorn states are Eqs. (A5) and (A6), respectively. As

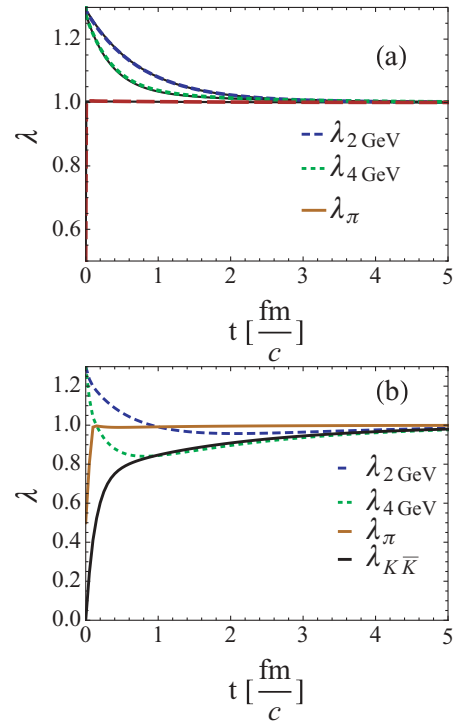

FIG. 31. (Color online) (a) Numerical and analytical results for the pions and Hagedorn states, where $\eta = 0.9$ at $T = 175$ MeV for $T_H = 176$ MeV when $\beta_i = 1.1$ and $\alpha = 0.9$. (b) Numerical results for the same initial conditions including $K\bar{K}$ pairs with $\phi = 0$.

with Stage 1, the evolution equation for the Hagedorn states is dictated by that of the pions.

Stage 3, that is, quasiequilibrium, begins once the pions and at least one species of Hagedorn resonances ($\tau_{7\,\mathrm{GeV}}$ is the shortest chemical equilibration time) has surpassed its equilibration time (τ_π and τ_i, respectively). To understand quasiequilibrium, we must use the effective pion number

$$\tilde{N}_\pi = N_\pi + \sum_i N_i \langle n_i \rangle \tag{A7}$$

because we need a variable that can observe the effects of both the pions and resonances. The effective pion number essentially includes the number of effective pions that each Hagedorn state could decay into. Thus, we start by taking the derivative of Eq. (A7) in terms of its fugacity

$$\begin{aligned}\dot{\tilde{\lambda}}_\pi &= \frac{1}{\tilde{N}_\pi^{\mathrm{eq}}}\left[N_\pi^{\mathrm{eq}}\dot{\lambda}_\pi + \sum_i N_i^{\mathrm{eq}}\dot{\lambda}_i\langle n_i\rangle\right] \\ &= \frac{\sum_i \Gamma_i N_i^{\mathrm{eq}}}{\tilde{N}_\pi^{\mathrm{eq}}}\left[\langle n_i\rangle \sum_n B_{i,n}\lambda_\pi^n - \sum_n B_{i,n} n \lambda_\pi^n\right].\end{aligned} \tag{A8}$$

Once again, we make the substitution $\lambda_\pi = 1 - \epsilon$ so that

$$\dot{\tilde{\epsilon}} = -\frac{1}{\tilde{N}_\pi^{\mathrm{eq}}}\sum_i \Gamma_i N_i^{\mathrm{eq}}\sigma_i^2\epsilon, \tag{A9}$$

where $\sigma_i^2 = \langle n_i^2\rangle - \langle n_i\rangle^2$ in the Gaussian distribution of our branching ratios. To relate ϵ and $\tilde{\epsilon}$, we return to Eq. (A7) and separate λ_i into a sum over the resonances in quasiequilibrium and one over the "freely" equilibrating resonances

$$\tilde{\lambda}_\pi = \frac{1}{\tilde{N}_\pi^{\mathrm{eq}}}\left[N_\pi^{\mathrm{eq}}\lambda_\pi + \sum_{\mathrm{QE}} N_i^{\mathrm{eq}}\langle n_i\rangle\lambda_i + \sum_{\mathrm{free}} N_i^{\mathrm{eq}}\langle n_i\rangle\lambda_i\right]. \tag{A10}$$

Because the pions reach quasiequilibrium first, that is, $\tau_\pi < \tau_i$ near T_c, we set the π rate equation in Eq. (16) equal to zero, which gives $\lambda_i \approx \frac{1}{\langle n_i\rangle}\sum_n B_{i,n} n \lambda_\pi^n$, so

$$\begin{aligned}\tilde{\lambda}_\pi \approx 1 &- \frac{\left(N_\pi^{\mathrm{eq}} + \sum_{\mathrm{QE}} N_i^{\mathrm{eq}}\langle n_i^2\rangle\right)\epsilon}{\tilde{N}_\pi^{\mathrm{eq}}} \\ &- \frac{\sum_{\mathrm{free}}\langle n_i\rangle\left(N_i^{\mathrm{eq}} - N_i^{\mathrm{eq}}\lambda_i\right)}{\tilde{N}_\pi^{\mathrm{eq}}}.\end{aligned} \tag{A11}$$

Equation (A11) then has the form $\tilde{\lambda}_\pi \approx 1 - \tilde{\epsilon}$, where

$$\tilde{\epsilon} = \frac{\left(N_\pi^{\mathrm{eq}} + \sum_{\mathrm{QE}} N_i^{\mathrm{eq}}\langle n_i^2\rangle\right)\epsilon}{\tilde{N}_\pi^{\mathrm{eq}}} + \frac{\sum_{\mathrm{free}}\langle n_i\rangle\left(N_i^{\mathrm{eq}} - N_i^{\mathrm{eq}}\lambda_i\right)}{\tilde{N}_\pi^{\mathrm{eq}}}. \tag{A12}$$

We can then solve for ϵ in Eq. (A12) and substitute ϵ into Eq. (A9), which in turn can be integrated. This leads us to the solution

$$\begin{aligned}\tilde{\epsilon} = \epsilon_j e^{-\frac{t-\tau_j}{\tau_\pi^{\mathrm{QE}}}} &+ \sum_{\mathrm{free}}\langle n_i\rangle N_i^{\mathrm{eq}} - \frac{\sum_i \Gamma_i N_i^{\mathrm{eq}}\sigma_i^2}{\tilde{N}_\pi^{\mathrm{eq}}\sum_{\mathrm{QE}} N_i\langle n_i^2\rangle} \\ &\times \sum_{\mathrm{free}} N_i^{\mathrm{eq}}\langle n_i\rangle e^{-\frac{t-\tau_j}{\tau_\pi^{\mathrm{QE}}}}\int_0^t e^{\frac{x-\tau_j}{\tau_\pi^{\mathrm{QE}}}}\lambda_i(x)dx,\end{aligned} \tag{A13}$$

where j stands for the latest resonance to reach chemical equilibrium at that point in time and

$$\tau_\pi^{\mathrm{QE}} \equiv \frac{N_\pi^{\mathrm{eq}}}{\sum_i \Gamma_i N_i^{\mathrm{eq}}\sigma_i^2} + \frac{\sum_{QE} N_i^{\mathrm{eq}}\langle n_i^2\rangle}{\sum_i \Gamma_i N_i^{\mathrm{eq}}\sigma_i^2} \tag{A14}$$

is the quasiequilibrium time. Clearly, once all the Hagedorn states have reached chemical equilibrium, then j symbolizes the resonance of $M = 2$ GeV, because it is the slowest Hagedorn state to equilibrate. The sums over "free" is the sum over the Hagedorn states that have not yet surpassed their respective chemical equilibrium time, τ_i. Once $\tau_{2\,\mathrm{GeV}}$ is reached, those sums equal zero. Therefore, after $\tau_{2\,\mathrm{GeV}}$, all that remains is

$$\tilde{\epsilon} = \epsilon_{2\,\mathrm{GeV}} e^{-\frac{t-\tau_{2\,\mathrm{GeV}}}{\tau_\pi^{\mathrm{QE}}}}, \tag{A15}$$

where τ_π^{QE} is shown in Table I. Finally, we rewrite Eq. (A15) in terms of the pion evolution equation

$$\lambda_\pi = 1 - (1-\kappa)e^{-\frac{t-\tau_{2\,\mathrm{GeV}}}{\tau_\pi^{\mathrm{QE}}}}, \tag{A16}$$

where $\kappa = \lambda_\pi(\tau_{2\,\mathrm{GeV}})$.

Because the resonance equation depends on the population of the pions, we substitute Eq. (A16) into the Hagedorn resonance rate equation in Eq. (16), assuming the pions are near equilibrium [i.e., we use the approximation $\lambda = 1 - \epsilon$ and $(1-\epsilon)^n \approx 1 - n\epsilon$],

$$\begin{aligned}\lambda_i = &\left[\theta_i - 1 + \frac{\tau_\pi^{\mathrm{QE}}}{\tau_\pi^{\mathrm{QE}} - \tau_i}\langle n_i\rangle(1-\kappa)\right]e^{-\frac{t-\tau_{2\,\mathrm{GeV}}}{\tau_i}} \\ &+ 1 - \frac{\tau_\pi^{\mathrm{QE}}}{\tau_\pi^{\mathrm{QE}} - \tau_i}\langle n_i\rangle(1-\kappa)e^{-\frac{t-\tau_j}{\tau_\pi^{\mathrm{QE}}}},\end{aligned} \tag{A17}$$

where $\theta_i = \lambda_i(\tau_{2\,\mathrm{GeV}})$. Thus, for Stage 3 the population equations for the pions and the Hagedorn states are Eqs. (A16) and (A17) so long as $t \geqslant \tau_{2\,\mathrm{GeV}}$.

Figure 31 reveals a remarkable close fit with our numerical results for $T = 175$ MeV; that is, $T < T_H$. Thus, the quasichemical equilibrium time, τ^{QE}, depends only on Γ_i, $\langle n_i\rangle$, σ_i^2, and N^{eq}, which is temperature dependent, but not on our initial conditions. As mentioned in the text, though, τ^{QE} includes many nonlinear effects that only occur close to the chemical equilibrium. Thus, the more appropriate time scale is τ_π^0 to describe the dynamics.

We also see from Fig. 31 that when $K\bar{K}$ pairs are included the pions and Hagedorn resonances equilibrate in roughly the same amount of time, which implies that our analytical solution can still be approximately applied when $K\bar{K}$ pairs are present.

[1] P. Koch, B. Muller, and J. Rafelski, Phys. Rep. **142**, 167 (1986).

[2] R. Rapp and E. V. Shuryak, Phys. Rev. Lett. **86**, 2980 (2001).

[3] C. Greiner, AIP Conf. Proc. **644**, 337 (2003); Heavy Ion Phys. **14**, 149 (2001); C. Greiner and S. Leupold, J. Phys. G **27**, L95 (2001).
[4] P. Braun-Munzinger *et al.*, Phys. Lett. B **344**, 43 (1995); **365**, 1 (1996); Eur. Phys. J. C **2**, 351, (1998); P. Braun-Munzinger, I. Heppe, and J. Stachel, Phys. Lett. B **465**, 15 (1999).
[5] J. I. Kapusta and I. Shovkovy, Phys. Rev. C **68**, 014901 (2003); J. I. Kapusta, J. Phys. G **30**, S351 (2004).
[6] P. Huovinen and J. I. Kapusta, Phys. Rev. C **69**, 014902 (2004).
[7] R. Stock, Phys. Lett. B **456**, 277 (1999); PoS C **POD2006**, 040 (2006).
[8] U. Heinz and G. Kestin, PoS C **POD2006**, 038 (2006).
[9] P. Braun-Munzinger, J. Stachel, and C. Wetterich, Phys. Lett. B **596**, 61 (2004).
[10] C. Greiner *et al.*, J. Phys. G **31**, S725 (2005).
[11] J. Noronha-Hostler, C. Greiner, and I. A. Shovkovy, Phys. Rev. Lett. **100**, 252301 (2008).
[12] J. Noronha-Hostler, J. Noronha, H. Ahmad, I. Shovkovy, and C. Greiner, Nucl. Phys. A **830**, 745c (2009); J. Noronha-Hostler, C. Greiner, and I. Shovkovy, Eur. Phys. J. ST **155**, 61 (2008); Proceedings of 45th International Winter Meeting on Nuclear Physics, Bormio, Italy, 14–21 January 2007, arXiv:nucl-th/0703079.
[13] J. Noronha-Hostler, J. Noronha, and C. Greiner (to appear in Phys. Rev. Lett.).
[14] P. K. Kovtun, D. T. Son, and A. O. Starinets, Phys. Rev. Lett. **94**, 111601 (2005).
[15] D. Kharzeev and K. Tuchin, J. High Energy Phys. 09 (2008) 093.
[16] J. Noronha-Hostler, H. Ahmad, J. Noronha, and C. Greiner (to be published in Phys. Rev. C), arXiv:0906.3960v1 [nucl-th].
[17] Y. Aoki, Z. Fodor, S. D. Katz, and K. K. Szabo, J. High Energy Phys. 01 (2006) 089; Phys. Lett. B **643**, 46 (2006).
[18] M. Cheng *et al.*, Phys. Rev. D **77**, 014511 (2008).
[19] A. Bazavov *et al.*, Phys. Rev. D **80**, 014504 (2009).
[20] R. Hagedorn, Nuovo Cimento Suppl. **6**, 311 (1968); **3**, 147 (1965).
[21] W. Broniowski, W. Florkowski, and L. Y. Glozman, Phys. Rev. D **70**, 117503 (2004), arXiv:hep-ph/0407290.
[22] K. A. Bugaev, V. K. Petrov, and G. M. Zinovjev, arXiv:0801.4869 [hep-ph].
[23] L. G. Moretto, L. Phair, K. A. Bugaev, and J. B. Elliott, PoS C **POD2006**, 037 (2006); L. G. Moretto, K. A. Bugaev, J. B. Elliott, and L. Phair, arXiv:nucl-th/0601010; Proceedings of 3rd World Consensus Initiative (WCI3), College Station, Texas, 12–16 February 2005, arXiv:hep-ph/0511180.
[24] I. Zakout, C. Greiner, and J. Schaffner-Bielich, Nucl. Phys. A **781**, 150 (2007); I. Zakout and C. Greiner, Phys. Rev. C **78**, 034916 (2008); L. Ferroni and V. Koch, *ibid.* **79**, 034905 (2009).
[25] J. R. Ellis and K. Geiger, Phys. Rev. D **54**, 1967 (1996).
[26] J. I. Kapusta and K. A. Olive, Nucl. Phys. A **408**, 478 (1983).
[27] D. H. Rischke, M. I. Gorenstein, H. Stoecker, and W. Greiner, Z. Phys. C **51**, 485 (1991).
[28] S. A. Bass *et al.*, Prog. Part. Nucl. Phys. **41**, 255 (1998); M. Bleicher *et al.*, J. Phys. G **25**, 1859 (1999).
[29] S. Pal and P. Danielewicz, Phys. Lett. B **627**, 55 (2005).
[30] F. M. Liu, K. Werner, and J. Aichelin, Phys. Rev. C **68**, 024905 (2003); F. M. Liu, J. Aichelin, M. Bleicher, and K. Werner, J. Phys. G **30**, S589 (2004); Phys. Rev. C **69**, 054002 (2004).
[31] F. Becattini and L. Ferroni, Eur. Phys. J. C **38**, 225 (2004).
[32] M. Beitel, J. Noronha-Hostler, and C. Greiner (unpublished).
[33] I. Senda, Phys. Lett. B **263**, 270 (1991); F. Lizzi and I. Senda, Nucl. Phys. B **359**, 441 (1991); Phys. Lett. B **244**, 27 (1990).
[34] S. Eidelman *et al.*, Phys. Lett. B **592**, 1 (2004).
[35] C. Spieles, H. Stoecker, and C. Greiner, Eur. Phys. J. C **2**, 351 (1998); C. Greiner, D. H. Rischke, H. Stocker, and P. Koch, Phys. Rev. D **38**, 2797 (1988); C. Greiner and H. Stocker, *ibid.* **44**, 3517 (1991).
[36] I. G. Bearden *et al.* (BRAHMS Collaboration), Phys. Rev. Lett. **94**, 162301 (2005).
[37] C. Greiner, C. Gong, and B. Muller, Phys. Lett. B **316**, 226 (1993).